# Chapter 6
# RANS Simulations of Premixed Turbulent Flames

**Andrei N. Lipatnikov**

**Abstract** While Reynolds-Averaged Navier-Stokes (RANS) simulations are widely used in applied research into premixed turbulent burning in spark ignition piston engines and gas-turbine combustors, fundamental challenges associated with modeling various unclosed terms in the RANS transport equations that describe premixed flames have not yet been solved. These challenges stem from two kinds of phenomena. First, thermal expansion due to heat release in combustion reactions affects turbulent flow and turbulent transport. Such effects manifest themselves in the so-called counter gradient turbulent transport, flame-generated turbulence, hydrodynamic instability of premixed combustion, etc. Second, turbulent eddies wrinkle and stretch reaction zones, thus, increasing their surface area and changing their local structure. Both the former effects, i.e. the influence of combustion on turbulence, and the latter effects, i.e. the influence of turbulence on combustion, are localized to small scales unresolved in RANS simulations and, therefore, require modeling. In the present chapter, the former effects, their physical mechanisms and manifestations, and approaches to modeling them are briefly overviewed, while discussion of the latter effects is more detailed. More specifically, the state-of-the-art of RANS modeling of the influence of turbulence on premixed combustion is considered, including widely used approaches such as models that deal with a transport equation for the mean Flame Surface Density or the mean Scalar Dissipation Rate. Subsequently, the focus of discussion is placed on phenomenological foundations, closed equations, qualitative features, quantitative validation, and applications of the so-called Turbulent Flame Closure (TFC) model and its extension known as Flame Speed Closure (FSC) model.

**Keywords** Turbulent combustion · Premixed turbulent flames · Modelling RANS simulations · validation

A. N. Lipatnikov (✉)
Chalmers University of Technology, 41296 Gothenburg, Sweden
e-mail: lipatn@chalmers.se



S. De et al. (eds.), *Modeling and Simulation of Turbulent Combustion*, Energy, Environment, and Sustainability, https://doi.org/10.1007/978-981-10-7410-3_6

## 6.1 Introduction

In this chapter, the problem of unsteady multidimensional numerical simulations of premixed turbulent combustion is stated, transport equations that describe variations of mean (Favre-averaged) mixture and flow characteristics in turbulent flames are introduced, and fundamental challenges associated with applications of these equations are discussed. Various approaches to modeling unknown terms in the Favre-averaged transport equations are briefly overviewed, followed by a detailed discussion of foundations, equations, qualitative features, quantitative validation, and engine applications of the so-called Turbulent Flame Closure (TFC) model, which is implemented into most commercial CFD codes, as well as its extension known as Flame Speed Closure (FSC) model.

## 6.2 Mathematical Background

The goal of this section is to introduce transport equations that RANS models of premixed turbulent combustion deal with.

### *6.2.1 General Transport Equations*

A general set of transport equations that model reacting flows is discussed in detail elsewhere (Williams 1985). When modeling premixed turbulent combustion, a less general set of transport equations is commonly used by invoking the following simplifications (Libby and Williams 1994)

- The molecular mass and heat fluxes are approximated by Fick's and Fourier's laws, respectively.
- The Soret and Dufour effects, pressure gradient diffusion, and bulk viscosity are negligible.
- There is no body force.
- The Mach number is much less than unity.
- The mixture is an ideal gas, i.e.,

$$pM = \rho R^o T, \tag{6.1}$$

where $p$, $\rho$, and $T$ are the pressure, density, and temperature, respectively, $M$ is the molecular weight of the mixture, and $R^o$ is the universal gas constant.

Under the above assumptions, combustion of gases is modeled by the following transport equations.

Mass conservation (continuity) equation reads

$$\frac{\partial \rho}{\partial t} + \frac{\partial}{\partial x_j}\left(\rho u_j\right) = 0, \tag{6.2}$$

where $t$ is the time, $x_j$ and $u_j$ are the spatial coordinates and flow velocity components, respectively. Henceforth, the summation convention applies for a repeated index that indicates the coordinate axis, e.g., the repeated index $j$ in Eq. (6.2), if the opposite is not stated.

Momentum conservation (Navier–Stokes) equation reads

$$\frac{\partial}{\partial t}\left(\rho u_i\right) + \frac{\partial}{\partial x_j}\left(\rho u_i u_j\right) = \frac{\partial \tau_{ij}}{\partial x_j} - \frac{\partial p}{\partial x_i}, \tag{6.3}$$

where

$$\tau_{ij} = \mu\left(\frac{\partial u_i}{\partial x_j} + \frac{\partial u_j}{\partial x_i} - \frac{2}{3}\frac{\partial u_l}{\partial x_l}\delta_{ij}\right) \tag{6.4}$$

is the viscous stress tensor, $\delta_{ij}$ is the Kronecker delta, and the dynamic molecular viscosity $\mu$ depends on pressure, temperature, and mixture composition. Methods for evaluating the viscosity and other molecular transport coefficients (e.g., the mass diffusivity $D_k$ of species $k$ in a mixture or the heat diffusivity $\kappa$ of the mixture) are discussed elsewhere (Giovangigli 1999; Hirschfelder et al. 1954). In the present chapter, these transport coefficients are considered to be known functions of pressure and temperature for each particular mixture.

Species mass conservation equations read

$$\frac{\partial}{\partial t}\left(\rho Y_k\right) + \frac{\partial}{\partial x_j}\left(\rho u_j Y_k\right) = \frac{\partial}{\partial x_j}\left(\rho D_k \frac{\partial Y_k}{\partial x_j}\right) + \dot{\omega}_k, \tag{6.5}$$

where $Y_k$ is the mass fraction of species $k$, $\dot{\omega}_k$ is the mass rate of creation ($\dot{\omega}_k > 0$) or consumption ($\dot{\omega}_k < 0$) of the species $k$, and the summation convention does not apply for the species index $k$. If $N$ species $\mathscr{S}_k$ ($k = 1, \ldots, N$) participate in $M$ reactions

$$\sum_{k=1}^{N} a_{km}\mathscr{S}_k \rightleftharpoons \sum_{k=1}^{N} b_{km}\mathscr{S}_k, \tag{6.6}$$

where $m = 1, \ldots, M$, then, the rate

$$\dot{\omega}_k = \sum_{m=1}^{M} \dot{\omega}_{km}, \tag{6.7}$$

where

$$\dot{\omega}_{km} = a_{km} k_{b,m} \rho^{b_m} \prod_{n=1}^{N} Y_n^{b_{nm}} - b_{km} k_{f,m} \rho^{a_m} \prod_{n=1}^{N} Y_n^{a_{nm}}, \tag{6.8}$$

$a_m = \sum_{k=1}^{N} a_{km}$ and $b_m = \sum_{k=1}^{N} b_{km}$ are orders of the forward and backward reactions $m$, respectively, and the forward and backward reaction rates $k_{f,m}$ and $k_{b,m}$, respectively, have dimensions of $(\mathrm{kg/m^3})^{a_m - 1}\mathrm{s}^{-1}$ and $(\mathrm{kg/m^3})^{b_m - 1}\mathrm{s}^{-1}$, respectively. The reaction rates are commonly modeled as follows:

$$k_{f,m} = B_{f,m} T^{n_{f,m}} \exp\left(-\frac{\Theta_{f,m}}{T}\right), \qquad k_{b,m} = B_{b,m} T^{n_{b,m}} \exp\left(-\frac{\Theta_{b,m}}{T}\right), \tag{6.9}$$

where $B_{f,m}, n_{f,m}$ and $B_{b,m}, n_{b,m}$ are constants of the forward and backward reactions $m$, respectively, $\Theta_{f,m}$ and $\Theta_{b,m}$ are their activation temperatures, with a ratio of $\Theta_{f,m}/T$ being large for many important combustion reactions.

In premixed flames, energy conservation can be modeled using a transport equation for specific mixture enthalpy $h$, specific mixture internal energy $e = h - p/\rho$, or temperature. For instance, the enthalpy conservation equation reads

$$\frac{\partial}{\partial t}(\rho h) + \frac{\partial}{\partial x_j}\left(\rho u_j h\right) = \frac{\partial p}{\partial t} + \frac{\partial}{\partial x_j}\left[\frac{\mu}{Pr}\frac{\partial h}{\partial x_j} + \mu \sum_{k=1}^{N}\left(\frac{1}{Sc_k} - \frac{1}{Pr}\right) h_k \frac{\partial Y_k}{\partial x_j}\right] - q_R, \tag{6.10}$$

where $Pr = \mu/\rho\kappa = \nu/\kappa$ and $Sc_k = \mu/\rho D_k$ are the Prandtl and Schmidt numbers, respectively, $\nu = \mu/\rho$ is the molecular kinematic viscosity, $q_R$ is radiative heat loss,

$$h_k = \int_{T_0}^{T} c_{p,k} dT + \Delta h_k \tag{6.11}$$

is the specific enthalpy of species $k$ per unit mass,

$$h = \sum_{k=1}^{N} Y_k h_k = \sum_{k=1}^{N} \int_{T_0}^{T} c_{p,k} dT + \sum_{k=1}^{N} Y_k \Delta h_k = \int_{T_0}^{T} c_p dT + \sum_{k=1}^{N} Y_k \Delta h_k \tag{6.12}$$

is the specific mixture enthalpy per unit mass, $\Delta h_k$ is the enthalpy of species $k$ at a reference temperature $T_0$, and $c_p = \sum_{k=1}^{N} c_{p,k}$ is the specific heat of the mixture at constant pressure. In the rest of this chapter, adiabatic burning will be considered, i.e., $q_R = 0$ if the opposite is not specified.

If the specific heats $c_{p,k}$ are equal to the same $c_p$ for all species, then, the following temperature transport equation

$$c_p \frac{\partial}{\partial t}(\rho T) + c_p \frac{\partial}{\partial x_j}\left(\rho u_j T\right) = \frac{\partial p}{\partial t} + \frac{\partial}{\partial x_j}\left(\lambda \frac{\partial T}{\partial x_j}\right) - \sum_{k=1}^{N} (\Delta h_k \dot{\omega}_k) \tag{6.13}$$

can be obtained by substituting Eq. (6.12) into Eq. (6.10) and using Eq. (6.5). Here, $\lambda = \rho c_p \kappa$ is the heat conductivity of the mixture. For simulations of turbulent combustion, Eq. (6.10) is more suitable than Eq. (6.13), because the latter equation involves highly nonlinear source term $\sum_{k=1}^{N} (\Delta h_k \dot{\omega}_k)$, whose magnitude fluctuates strongly in a premixed turbulent flame.

Equations (6.1)–(6.12) can be integrated numerically to study a 1D laminar flame. Such a research method is routinely used today and a number of advanced software packages are available on the market.

If Eqs. (6.1)–(6.12) are numerically solved to simulate a 3D turbulent flame, such computations should be performed using a fine mesh that resolves both the smallest turbulent eddies and spatial variations of species within thin reaction zones. Such a research method is known as Direct Numerical Simulation (DNS).

DNS is an expensive numerical tool and its applications are mainly limited to simple model problems. Even in a constant-density non-reacting case, the size of a numerical mesh required for 3D DNS study of a turbulent flow is on the order of $\mathrm{Re}_t^3$ (Pope 2000), because (i) a ratio of length scales of the largest and smallest eddies in such a flow is on the order of $\mathrm{Re}_t^{3/4}$ and (ii) time step $\Delta t$ is typically proportional to the mesh step $\Delta x \propto \mathrm{Re}_t^{3/4}$ in such simulations. Therefore, a DNS of a flow characterized by a really high turbulent Reynolds number $\mathrm{Re}_t = u'L/\nu$ is still a challenging task. Here, $u'$ and $L$ designate rms velocity and an integral length scale of turbulence, respectively.

In the case of premixed combustion, the main challenge consists not only of a significant increase in a number of transport equations to be solved, i.e., $O(N)$ Eq. (6.5), but also (and mainly) in extension of the range of spatial scales to be resolved. Accordingly, the majority of contemporary DNS studies of premixed turbulent flames deal with moderate $\mathrm{Re}_t$ (typically, well below 1000) and with comparable values of $L$ and laminar flame thickness in order for ranges of spatial scales associated with combustion and turbulence to well overlap. A 3D DNS study of a turbulent premixed flame characterized by a large (when compared to the laminar flame thickness) length scale $L$ and, hence, by $\mathrm{Re}_t = O(1000)$ or higher is still an unfeasible task. Accordingly, such flames are numerically modeled invoking simplified approaches such as Reynolds-Averaged Navier Stokes (RANS) or Large Eddy Simulation (LES). The former research tool will be discussed in the rest of the present chapter.

### 6.2.2 *Favre-Averaged Transport Equations for First Moments*

RANS approach is based on the decomposition of any (scalar, vector, tensor, etc.) field $q(\mathbf{x}, t)$ into mean $\bar{q}(\mathbf{x}, t)$ and fluctuating $q'(\mathbf{x}, t) \equiv q(\mathbf{x}, t) - \bar{q}(\mathbf{x}, t)$ fields. By definition $\overline{\bar{q}(\mathbf{x}, t)} = \bar{q}(\mathbf{x}, t)$ and, hence, $\overline{q'(\mathbf{x}, t)} = \bar{q}(\mathbf{x}, t) - \overline{\bar{q}(\mathbf{x}, t)} = 0$. The mean field $\bar{q}(\mathbf{x}, t)$ can be determined by averaging the field $q(\mathbf{x}, t)$ over a sufficiently long time interval, surface, or an ensemble of statistically equivalent realizations of a stochastic process. Taking average over time is most suitable in the case of a statistically stationary process, e.g., burning behind a flame-holder. In such a case, $\bar{q}$ does not depend on time. Taking average over a surface is most suitable in the case of a statistically 1D process, e.g., a statistically planar 1D flame addressed in a DNS or a spherical flame kernel growing in homogeneous turbulence after spark ignition. In

such a case, $\bar{q}$ depends on a single spatial coordinate, distance $x$ normal to the mean flame position or radial coordinate $r$, respectively. Ensemble-averaged quantities are commonly used in investigations of transient and spatially nonuniform mean flows, e.g., combustion in a chamber of a piston engine. In such a case, $q(\mathbf{x}, t)$ is an ensemble of fields. These three methods of taking an average are considered to be fundamentally equivalent, i.e., if the two or three methods can be applied to the same field $q(\mathbf{x}, t)$ or the same ensemble of fields, the obtained mean fields $\bar{q}(\mathbf{x}, t)$ should be the same.

If $\rho(\mathbf{x}, t) = \bar{\rho}(\mathbf{x}, t) + \rho'(\mathbf{x}, t)$ and $\mathbf{u}(\mathbf{x}, t) = \bar{\mathbf{u}}(\mathbf{x}, t) + \mathbf{u}'(\mathbf{x}, t)$ are substituted into Eq. (6.2) and the obtained transport equation is averaged, then, we arrive at

$$0 = \frac{\partial \bar{\rho}}{\partial t} + \frac{\partial}{\partial x_j}\left(\bar{\rho}\bar{u}_j + \overline{\rho' u_j'}\right), \tag{6.14}$$

because $\overline{ab} = \overline{(\bar{a} + a')(\bar{b} + b')} = \bar{a}\bar{b} + \overline{a'}\bar{b} + \overline{b'}\bar{a} + \overline{a'b'} = \bar{a}\bar{b} + \overline{a'b'}$ for arbitrary quantities $a$ and $b$. In the following, dependencies of various flow and mixture characteristics on the spatial coordinates $\mathbf{x}$ and time $t$ will often be skipped for brevity. Nevertheless, when introducing new flame characteristics, such dependencies will sometimes be specified in the beginning and, then, will be skipped.

Equation (6.14) involves a second moment $\overline{\rho' u_j'}$, i.e., a correlation of fluctuating density and velocity fields, which should be modeled. This problem can be circumvented by introducing Favre-averaged mass-weighted quantities as follows; $\tilde{q} \equiv \overline{\rho q}/\bar{\rho}$ and $q'' \equiv q - \tilde{q}$. By definition, $\tilde{q''} = \overline{\rho q''} = 0$. If $\mathbf{u} = \tilde{\mathbf{u}} + \mathbf{u}''$ is substituted into Eq. (6.2) and the obtained transport equation is averaged using the Reynolds method, then, we arrive at

$$\frac{\partial \bar{\rho}}{\partial t} + \frac{\partial}{\partial x_j}\left(\bar{\rho}\tilde{u}_j\right) = 0, \tag{6.15}$$

because $\overline{\rho \mathbf{u}} = \bar{\rho}\tilde{\mathbf{u}}$ by definition. The Favre-averaged transport Eq. (6.15) involves less number of terms when compared to the Reynolds-averaged transport Eq. (6.14) and a similar result can be obtained by averaging other transport equations. For this reason, RANS models of turbulent combustion deal with the Favre-averaged transport equations.

Substitution of $u_i = \tilde{u}_i + u_i''$ and $u_j = \tilde{u}_j + u_j''$ into the Navier–Stokes Eq. (6.3), followed by averaging, yields

$$\frac{\partial}{\partial t}\left(\bar{\rho}\tilde{u}_i\right) + \frac{\partial}{\partial x_j}\left(\bar{\rho}\tilde{u}_i\tilde{u}_j\right) = -\frac{\partial}{\partial x_j}\overline{\rho u_i'' u_j''} + \frac{\partial \bar{\tau}_{ij}}{\partial x_j} - \frac{\partial \bar{p}}{\partial x_i}, \tag{6.16}$$

because $\overline{\rho ab} = \overline{\rho(\tilde{a} + a'')(\tilde{b} + b'')} = \bar{\rho}\tilde{a}\tilde{b} + \overline{\rho a''}\tilde{b} + \overline{\rho b''}\tilde{a} + \overline{\rho a'' b''} = \bar{\rho}\tilde{a}\tilde{b} + \overline{\rho a'' b''}$ for arbitrary quantities $a$ and $b$.

Using a similar method, we arrive at the following Favre-averaged transport equations for species mass fractions

$$\frac{\partial}{\partial t}\left(\bar{\rho}\tilde{Y}_k\right)+\frac{\partial}{\partial x_j}\left(\bar{\rho}\tilde{u}_j\tilde{Y}_k\right)=-\frac{\partial}{\partial x_j}\overline{\rho u_j''Y_k''}+\frac{\partial}{\partial x_j}\left(\overline{\rho D_k\frac{\partial Y_k}{\partial x_j}}\right)+\bar{\dot{\omega}}_k \tag{6.17}$$

and specific mixture enthalpy

$$\frac{\partial}{\partial t}\left(\bar{\rho}\tilde{h}\right)+\frac{\partial}{\partial x_j}\left(\bar{\rho}\tilde{u}_j\tilde{h}\right)=-\frac{\partial}{\partial x_j}\overline{\rho u_j''h''}+\frac{\partial\bar{p}}{\partial t}$$
$$+\overline{\frac{\partial}{\partial x_j}\left[\frac{\mu}{Pr}\frac{\partial h}{\partial x_j}+\mu\sum_{k=1}^{N}\left(\frac{1}{Sc_k}-\frac{1}{Pr}\right)h_k\frac{\partial Y_k}{\partial x_j}\right]}. \tag{6.18}$$

Finally, the Favre-averaged ideal gas state Eq. (6.1) reads

$$\overline{pM}=R^o\bar{\rho}\tilde{T}. \tag{6.19}$$

If the Mach number is much less than unity, then, fluctuations and spatial variations in the pressure may be neglected in Eq. (6.19) when compared to the mean pressure (Majda and Sethian 1985). Therefore, symbol $p$ in Eq. (6.19) designates pressure averaged over the entire combustion chamber. Accordingly, Eq. (6.19) reads $p\overline{M}=R^o\bar{\rho}\tilde{T}$ and allows us to evaluate the mean density, e.g., if the molecular wight $M$ is assumed to be constant.

## 6.3 Challenges of and Approaches to Premixed Turbulent Combustion Modeling Within RANS Framework

Equations (6.15)–(6.18) involve (i) terms that can be determined by solving these equations, e.g., the first moments $\bar{\rho}$, $\tilde{u}_i$, $\tilde{Y}_k$, and $\tilde{h}$ of the density, velocity, mass fraction, and enthalpy fields, and (ii) the so-called unclosed terms that cannot be determined by solving the transport Eqs. (6.15)–(6.18), e.g., turbulent Reynolds stresses $\overline{\rho u_i''u_j''}$, turbulent scalar fluxes $\overline{\rho u_j''Y_k''}$ and $\overline{\rho u_j''h''}$ or the mean reaction rates $\bar{\dot{\omega}}_k$. Accordingly, the number of unknowns is larger than the number of equations and the latter terms should be modeled. Model equations invoked for these purposes are commonly called closure relations.

The present section aims at briefly reviewing (i) various approaches to modeling the aforementioned unclosed terms and (ii) associated challenges. However, before considering such approaches and challenges, it is worth substantially simplifying the problem, because an analysis of $O(N)$ transport Eq. (6.17) is difficult if $N\gg 1$. This goal is commonly reached using the so-called combustion progress variable, as discussed in the next section.

### 6.3.1 Combustion Progress Variable

The vast majority of models for RANS simulations of premixed turbulent flames are based on an assumption that the state of the mixture in a premixed flame can be characterized with a single combustion progress variable $c$ in the adiabatic iso-baric[1] case (e.g., an open flame) or by two variables $c$ and $h$ if heat losses are substantial or/and the pressure depends on time (e.g. combustion in piston engines). For simplicity, in the rest of the present chapter, we will address the former (adiabatic iso-baric) case if the opposite is not stated.

The aforementioned assumption can be justified by invoking one of the following three approximations: (i) single-step chemistry and equidiffusive mixture, (ii) flamelet combustion regime, (iii) two-fluid flow. Each approximation offers an opportunity to significantly simplify the problem, but retain the basic physics of flame–turbulence interaction in the focus of consideration. Let us consider these three approximations in a more detailed manner.

#### 6.3.1.1 Single-Step Chemistry Approximation

If combustion chemistry is reduced to a single reaction

$$\Phi \mathrm{F} + St\mathrm{O} \rightarrow \mathrm{P}$$

and the Lewis number $Le_k = \kappa/D_k$ is equal to unity for fuel F and oxidant O, then, Eq. (6.5) reads

$$\frac{\partial}{\partial t}\left(\rho Y_F\right) + \frac{\partial}{\partial x_j}\left(\rho u_j Y_F\right) = \frac{\partial}{\partial x_j}\left(\rho D \frac{\partial Y_F}{\partial x_j}\right) - \dot{\omega} \tag{6.20}$$

and

$$\frac{\partial}{\partial t}\left(\rho Y_O\right) + \frac{\partial}{\partial x_j}\left(\rho u_j Y_O\right) = \frac{\partial}{\partial x_j}\left(\rho D \frac{\partial Y_O}{\partial x_j}\right) - St\dot{\omega} \tag{6.21}$$

for the fuel and oxidant, respectively. Here, $St$ is the mass stoichiometric coefficient and $\Phi$ is the equivalence ratio. A transport equation for the mass fraction of product P is not required, because $Y_P = Y_{F,u} - Y_F + St(Y_{O,u} - Y_O)$ due to mass conservation. Here, subscripts $u$ and $b$ designate fresh mixture and equilibrium combustion products, respectively.

If $Y_F = Y_{F,b} + y_F(Y_{F,u} - Y_{F,b})$ and $Y_O = Y_{O,b} + y_O(Y_{O,u} - Y_{O,b})$ are substituted into Eqs. (6.20) and (6.21), respectively, then, the transport equations for the normalized mass fractions of the fuel, $y_F$, and oxidant, $y_O$, are identical, because

[1] It is worth remembering that the pressure in a turbulent flow always fluctuates with time, but the magnitude of such fluctuations is much smaller than the mean pressure if the Mach number is low. Here, term "iso-baric case" means that the mean pressure does not depend on time.

$Y_{O,u} - Y_{O,b} = St(Y_{F,u} - Y_{F,b})$. The boundary conditions for $y_F$ and $y_O$ are also identical, i.e., $y_{F,u} = y_{O,u} = 1$ and $y_{F,b} = y_{O,b} = 0$. Consequently, the solutions $y_F(\mathbf{x}, t)$ and $y_O(\mathbf{x}, t)$ to the two equations should be the same in a general unsteady 3D case. Accordingly, if a combustion progress variable is defined as follows:

$$c = \frac{Y_F - Y_{F,u}}{Y_{F,b} - Y_{F,u}} = \frac{Y_O - Y_{O,u}}{Y_{O,b} - Y_{O,u}}, \tag{6.22}$$

then, the following transport equation

$$\frac{\partial}{\partial t}(\rho c) + \frac{\partial}{\partial x_j}\left(\rho u_j c\right) = \frac{\partial}{\partial x_j}\left(\rho D \frac{\partial c}{\partial x_j}\right) + \dot{\omega}_c \tag{6.23}$$

results from Eq. (6.20) or (6.21). Here, $\dot{\omega}_c = \dot{\omega}_F/(Y_{F,b} - Y_{F,u})$. By definition $c = 0$ and 1 in the unburned and burned gas, respectively.

Thus, the mixture composition is solely controlled by $c$. The temperature can be evaluated using Eq. (6.12), because the transport equation for the enthalpy simply reads

$$\frac{\partial}{\partial t}(\rho h) + \frac{\partial}{\partial x_j}\left(\rho u_j h\right) = \frac{\partial}{\partial x_j}\left(\lambda \frac{\partial h}{\partial x_j}\right) \tag{6.24}$$

and has a trivial solution of $h(\mathbf{x}, t) = \text{const}$ in the considered adiabatic, iso-baric, equidiffusive case. Furthermore, if the mixture specific heat $c_p$ is constant, as widely assumed when modeling premixed turbulent combustion, then, Eqs. (6.12) and (6.22) result straightforwardly in

$$c = \frac{T - T_u}{T_b - T_u}. \tag{6.25}$$

The mean molecular weight of the mixture is equal to

$$\overline{M} = \left(\frac{\overline{Y}_F}{M_F} + \frac{\overline{Y}_O}{M_O} + \frac{\overline{Y}_P}{M_P}\right)^{-1}, \tag{6.26}$$

where $M_F$, $M_O$, and $M_P$ are molecular weights of the fuel, oxidant, and product, respectively.

Thus, the combustion progress variable fully characterizes the mixture state in an arbitrary unsteady 3D flow provided that the invoked simplifications (single-step chemistry, $Le_F = Le_0 = 1$, $q_R = 0$, and the mean pressure $p$ does not depend on time) hold.

The Favre-averaged transport Eq. (6.23) reads

$$\frac{\partial}{\partial t}(\bar{\rho}\tilde{c}) + \frac{\partial}{\partial x_j}\left(\bar{\rho}\tilde{u}_j\tilde{c}\right) = -\frac{\partial}{\partial x_j}\overline{\rho u_j'' c''} + \frac{\partial}{\partial x_j}\overline{\left(\rho D \frac{\partial c}{\partial x_j}\right)} + \overline{\dot{\omega}_c} \tag{6.27}$$

To conclude this section, it is worth stressing the following points. The major goal of premixed turbulent combustion modeling consists in predicting the burning rate, which is commonly quantified by evaluating turbulent burning velocity $U_t$, i.e., burning rate per unit area of a mean flame surface, normalized using partial density of an appropriate reactant in unburned mixture. In various flames, this goal may be reached invoking a single-step chemistry and characterizing the mixture state in the flame with a single combustion progress variable provided that the used values of $\rho_b$, $T_b$, the laminar flame speed $S_L$ and thickness $\delta_L$ have been obtained in experiments or in simulations that dealt with detailed combustion chemistry.

For instance, Burluka et al. (2009) experimentally investigated expansion of various statistically spherical premixed turbulent flames in the well-known Leeds fan-stirred bomb. These authors studied not only burning of commonly used hydrocarbon–air mixtures, but also flames of di-t-butyl-peroxide (DTBP) decomposition, with such flames being associated with a much simpler chemistry when compared to combustion of hydrocarbons in the air. Nevertheless, similar dependencies of $U_t$ on the rms turbulent velocity $u'$ were obtained from both the hydrocarbon–air and DTBP flames, provided that they were characterized by approximately the same laminar flame speeds. These experimental data imply a minor effect of combustion chemistry on $U_t$.

Moreover, in a recent DNS study of premixed flames propagating in intense small-scale turbulence, Lapointe and Blanquart (2016) found that neither fuel formula nor chemical mechanism substantially affected computed turbulent burning velocity. Accordingly, they have concluded that "fuel consumption can be predicted with the knowledge of only a few global laminar flame properties" (Lapointe and Blanquart 2016). In another recent DNS study of lean methane–air turbulent flames under conditions relevant to Spark Ignition (SI) engines, Wang et al. (2017) compared results simulated using a single-step and a 13-species-reduced chemical mechanism. These authors have also concluded that the single-step "mechanism is adequate for predicting flame speed" (Wang et al. 2017).

Thus, in many cases, the use of a single combustion progress variable and a single-step chemistry appears to be basically adequate for analyzing the fundamentals of flame–turbulence interaction even if complex chemistry introduces new local effects, e.g., see Dasgupta et al. (2017). Nevertheless, combustion chemistry appears to play an important role under conditions associated with local combustion quenching e.g. due to heat losses, inflammable local mixture composition, strong local perturbations caused by turbulent eddies, etc.

#### 6.3.1.2 Flamelet Approximation

In the previous section, characterization of mixture state with a single combustion progress variable was obtained by considering an arbitrary flow, but significantly simplifying combustion chemistry and molecular transport model. The same result can also be obtained in the opposite case of complex combustion chemistry and an advanced model of molecular transport, but significantly simplified flow.

Indeed, the simplest paradigm of the influence of turbulence on premixed combustion consists in reducing this influence to wrinkling the surface of a thin inherently laminar flamelet whose structure is assumed to be close to the structure of the unperturbed planar 1D laminar flame (Bilger et al. 2005; Bray 1980, 1996; Lipatnikov 2012; Peters 2000; Poinsot and Veynante 2005). Accordingly, within the framework of such a paradigm, (i) the 1D laminar flame can be simulated using detailed chemistry and molecular transport models and (ii) results of such simulations can be tabulated in a form of $Y_k(c)$, $T(c)$, $\rho(c)$, etc., e.g., see a recent review paper by van Oijen et al. (2016). Subsequently, the state of the mixture in a premixed turbulent flame can be characterized with a single combustion progress variable $c$ and the aforementioned tables.

Such an approach was used in certain recent RANS studies of premixed turbulent combustion and is widely used in LES research into turbulent flames. However, it is worth remembering that the assumption that reaction zones retain the structure of weakly perturbed 1D laminar flames in a turbulent flow is very demanding and does not seem to hold even in weakly turbulent flames, e.g., see results (Lipatnikov et al. 2015b, 2017; Sabelnikov et al. 2016, 2017) of processing DNS data obtained from weakly turbulent flames that are well associated (Lipatnikov et al. 2015a) with the flamelet combustion regime. In the present author's opinion, this assumption distorts the basic physics of flame–turbulence interaction much stronger when the assumption of single-step chemistry does.

#### 6.3.1.3 Two-Fluid Approximation and BML Approach

To the best of the present author's knowledge, two-fluid approximation was introduced into the combustion literature by Prudnikov (1960, 1964). It is based on an assumption that unburned and burned gases are separated by an infinitely thin interface that propagates at the laminar flame speed $S_L$ with respect to the unburned mixture. Accordingly, the mean value of any mixture characteristic $q$ can be evaluated as follows:

$$\bar{q}(\mathbf{x}, t) = q_u \mathbb{P}_u(\mathbf{x}, t) + q_b \mathbb{P}_b(\mathbf{x}, t), \tag{6.28}$$

where $\mathbb{P}_u(\mathbf{x}, t)$ or $\mathbb{P}_b(\mathbf{x}, t)$ is the probability of finding the unburned or burned mixture, respectively, in point $\mathbf{x}$ at instant $t$ and $q_u$ or $q_b$ is the value of $q$ in the unburned or burned mixture, respectively. The latter value can be found by calculating the temperature and composition of the adiabatic equilibrium combustion products. In such calculations, the product composition may consist of a number of different species such as $H_2O$, $CO_2$, CO, $O_2$, $H_2$, $N_2$, OH, O, H, etc.

If we (i) introduce an indicator variable $I$, which is equal to zero and unity in the unburned and burned mixtures, respectively, and (ii) apply Eq. (6.28) to $I$, $(1 - I)$, $\rho I$, and $\rho(1 - I)$, then, we obtain

$$\bar{I} = \mathbb{P}_b, \qquad 1 - \bar{I} = \mathbb{P}_u, \qquad \bar{\rho}\tilde{I} = \overline{\rho I} = \rho_b \mathbb{P}_b, \qquad \bar{\rho}(1 - \tilde{I}) = \overline{\rho(1 - I)} = \rho_u \mathbb{P}_u, \tag{6.29}$$

respectively. Subsequently, the application of Eqs. (6.28) and (6.29) to $\rho Y_R$ and $\rho T$ yields

$$\bar{\rho}\tilde{Y}_R = \bar{\rho}(1 - \tilde{I})Y_{R,u} + \bar{\rho}\tilde{I}Y_{R,b}, \qquad \bar{\rho}\tilde{T} = \bar{\rho}(1 - \tilde{I})T_u + \bar{\rho}\tilde{I}T_b, \tag{6.30}$$

where subscript $R$ designates a reactant, e.g., fuel, oxygen, or product species. Consequently,

$$\tilde{I} = \frac{\tilde{Y}_F - Y_{F,u}}{Y_{F,b} - Y_{F,u}} = \frac{\tilde{Y}_O - Y_{O,u}}{Y_{O,b} - Y_{O,u}} = \frac{\tilde{T} - T_u}{T_b - T_u}, \tag{6.31}$$

i.e., the Favre-averaged value of the indicator function is equal to the Favre-averaged value of the combustion progress variable $c$ defined by Eq. (6.22) or (6.25). Finally, application of Eqs. (6.28) and (6.29) to $c$ and $(1 - c)$ yields

$$\bar{c} = \mathbb{P}_b = \bar{I}, \qquad 1 - \bar{c} = \mathbb{P}_u = 1 - \bar{I}, \tag{6.32}$$

i.e., the Reynolds-averaged value of the combustion progress variable is equal to the probability of finding combustion products and the indicator function $I$ can be substituted with $c$ in Eqs. (6.29)–(6.31).

In the particular case of single-step chemistry, the two-fluid approximation is associated with the limit of the infinitely fast reaction. Accordingly, the two-fluid approximation might be claimed to invoke an extra simplification when compared to the approximation of single-step chemistry. However, the former approximation offers an opportunity to use the temperature, density, and species mass fractions calculated for the equilibrium combustion products in the case of detailed chemistry.

Therefore, if the sum of the probabilities $\mathbb{P}_u$ and $\mathbb{P}_b$ is close to unity everywhere in a real flame, the two-fluid approach is capable of predicting mean mixture characteristics whose values within the reaction zones are of the same order or less than their values in the unburned or burned gas. However, the approach cannot be used to predict mean mass fractions of intermediate species, e.g., radicals, whose concentration is very low both in the unburned and burned mixtures. At first glance, this limitation of the two-fluid approximation appears to be a substantial drawback when compared to the flamelet approximation, which offers an opportunity to compute the mean mass fractions of intermediate species. However, to compute does not mean to predict. The use of the assumption of weak perturbations of the local flamelet structure when compared to the counterpart 1D laminar flame may yield wrong values of the mean mass fractions of the intermediate species if perturbations of the local flamelet structure are strong enough, as occurs in various flames. Accordingly, the present author cannot claim that the flamelet approximation is superior to the two-fluid approximation, at least within the RANS framework.

A bridge between the two-fluid and flamelet approximations was built by Bray (1980), Bray and Moss (1977), Bray et al. (1985) and Libby and Bray (1977, 1981) who developed the well-known BML approach by introducing the following Probability Density Function (PDF)

$$P(c,t,\mathbf{x}) = \alpha(t,\mathbf{x})\delta(c) + \beta(t,\mathbf{x})\delta(1-c) + \gamma(t,\mathbf{x})P_f(c,t,\mathbf{x}) \tag{6.33}$$

for the combustion progress variable defined using Eq. (6.22) written for the mass fraction of the deficient reactant, i.e., fuel in a lean mixture or oxygen in a rich mixture. Here, $\delta(c)$ and $\delta(1-c)$ are Dirac delta functions, $P_f(c,t,\mathbf{x})$ is an unknown PDF for $0 < c < 1$, i.e., $P_f(0,t,\mathbf{x}) = P_f(1,t,\mathbf{x}) = 0$, $\alpha(t,\mathbf{x})$ and $\beta(t,\mathbf{x})$ are the probabilities of finding unburned ($c = 0$) and burned ($c = 1$) mixture, respectively, while the probability $\gamma(t,\mathbf{x})$ of finding intermediate states ($0 < c < 1$) of the mixture is assumed to be much less than unity at any point $\mathbf{x}$ at any instant $t$. If $\gamma = 0$, the BML approach reduces to the two-fluid approximation. Alternatively, if $\gamma > 0$, a model for the intermediate PDF $P_f$ may be developed invoking the flamelet approximation (Bray et al. 2006).

Using Eq. (6.33), one can easily obtain Eqs. (6.29) and (6.30), where $I$ is substituted with $c$ and small terms on the order of $O(\gamma)$ are added on the RHSs of each equation. Moreover,

$$\bar{\rho} = (1-\bar{c})\rho_u + \bar{c}\rho_b + O(\gamma) = \rho_u - (\sigma-1)\rho_b\bar{c} + O(\gamma) = \rho_u - (\sigma-1)\bar{\rho}\tilde{c} + O(\gamma) \tag{6.34}$$

and, hence,

$$\bar{\rho} = \frac{\rho_u}{1+\tau\tilde{c}} + O(\gamma), \tag{6.35}$$

where $\sigma = \rho_u/\rho_b$ is the density ratio and $\tau = \sigma - 1$ is a heat-release factor.

The domain of validity of the BML approach is commonly characterized using the segregation factor

$$g = \frac{\overline{\rho c''^2}}{\bar{\rho}\tilde{c}(1-\tilde{c})}, \tag{6.36}$$

i.e., the closer $g$ to unity, the more accurate the BML approach is considered to be. Indeed, using Eq. (6.33), we have

$$\begin{aligned}\overline{\rho c''^2} &= \overline{\rho(c-\tilde{c})^2} = (1-\bar{c})\rho_u\tilde{c}^2 + \bar{c}\rho_b(1-\tilde{c})^2 + O(\gamma)\\ &= \bar{\rho}\left[(1-\tilde{c})\tilde{c}^2 + \tilde{c}(1-\tilde{c})^2\right] + O(\gamma) = \bar{\rho}\tilde{c}(1-\tilde{c}) + O(\gamma).\end{aligned} \tag{6.37}$$

Therefore, when $\overline{\rho c''^2} \to \bar{\rho}\tilde{c}(1-\tilde{c})$ and $g \to 1$, the magnitude of $O(\gamma)$-terms is asymptotically decreased and such unknown terms may be neglected if $g \approx 1$ and $\gamma \ll 1$. It is worth noting that Eqs. (6.34)–(6.37) can also be derived within the framework of the two-fluid approximation, but $O(\gamma)$-terms vanish in such a case.

In addition to the $c$-PDF given by Eq. (6.33), the BML approach deals with the following joint PDF

$$P(c,\mathbf{u},t,\mathbf{x}) = \alpha(t,\mathbf{x})P_u(\mathbf{u},t,\mathbf{x})\delta(c) + \beta(t,\mathbf{x})P_b(\mathbf{u},t,\mathbf{x})\delta(1-c) + \gamma(t,\mathbf{x})P_f(c,\mathbf{u},t,\mathbf{x}) \tag{6.38}$$

for the flow velocity vector $\mathbf{u}$ and the combustion progress variable $c$ at point $\mathbf{x}$ at instant $t$. Here, $P_u(\mathbf{u},t,\mathbf{x})$ and $P_b(\mathbf{u},t,\mathbf{x})$ are velocity PDFs conditioned on either the unburned or the burned mixture, respectively. Using Eq. (6.38), one can easily obtain the following equations:

$$\bar{\mathbf{u}} = \bar{\mathbf{u}}_u(1-\bar{c}) + \bar{\mathbf{u}}_b\bar{c} + O(\gamma), \tag{6.39}$$

$$\tilde{\mathbf{u}} = \bar{\mathbf{u}}_u(1-\tilde{c}) + \bar{\mathbf{u}}_b\tilde{c} + O(\gamma), \tag{6.40}$$

$$\overline{\rho\mathbf{u}''c''} = \overline{\rho(\mathbf{u}-\tilde{\mathbf{u}})(c-\tilde{c})} = (1-\bar{c})\rho_u(\bar{\mathbf{u}}_u-\tilde{\mathbf{u}})(-\tilde{c}) + \bar{c}\rho_b(\bar{\mathbf{u}}_b-\tilde{\mathbf{u}})(1-\tilde{c}) + O(\gamma)$$
$$= \bar{\rho}\left[-(1-\tilde{c})\tilde{c}(\bar{\mathbf{u}}_u-\tilde{\mathbf{u}}) + \tilde{c}(1-\tilde{c})(\bar{\mathbf{u}}_b-\tilde{\mathbf{u}})\right] + O(\gamma) = \bar{\rho}\tilde{c}(1-\tilde{c})\left(\bar{\mathbf{u}}_b-\bar{\mathbf{u}}_u\right) + O(\gamma), \tag{6.41}$$

$$\begin{aligned}\rho_u\overline{\mathbf{u}''} = \rho_u\overline{(\mathbf{u}-\tilde{\mathbf{u}})} &= (1-\bar{c})\rho_u(\bar{\mathbf{u}}_u-\tilde{\mathbf{u}}) + \bar{c}\rho_u(\bar{\mathbf{u}}_b-\tilde{\mathbf{u}}) + O(\gamma)\\ &= (1-\tilde{c})\bar{\rho}\tilde{c}(\bar{\mathbf{u}}_u-\bar{\mathbf{u}}_b) + \tilde{c}\sigma\bar{\rho}(1-\tilde{c})(\bar{\mathbf{u}}_b-\bar{\mathbf{u}}_u) + O(\gamma)\\ &= (\sigma-1)\bar{\rho}\tilde{c}(1-\tilde{c})(\bar{\mathbf{u}}_b-\bar{\mathbf{u}}_u) + O(\gamma) = \tau\overline{\rho\mathbf{u}''c''} + O(\gamma),\end{aligned} \tag{6.42}$$

$$\overline{\rho\mathbf{u}''\mathbf{u}''} = \bar{\rho}(1-\tilde{c})\overline{(\mathbf{u}'\mathbf{u}')}_u + \bar{\rho}\tilde{c}\overline{(\mathbf{u}'\mathbf{u}')}_b + \bar{\rho}\tilde{c}(1-\tilde{c})(\bar{\mathbf{u}}_b-\bar{\mathbf{u}}_u)(\bar{\mathbf{u}}_b-\bar{\mathbf{u}}_u) + O(\gamma). \tag{6.43}$$

Here, $\bar{\mathbf{u}}_u$ and $\bar{\mathbf{u}}_b$ are the velocity vectors conditioned to the unburned and burned mixture respectively, i.e.

$$\begin{aligned}\bar{\mathbf{u}}_u(\mathbf{x},t) &= \int_0^{\varepsilon}\left[\iiint \mathbf{u}P(c,\mathbf{u},\mathbf{x},t)d\mathbf{u}\right]dc,\\ \bar{\mathbf{u}}_b(\mathbf{x},t) &= \int_{1-\varepsilon}^{1}\left[\iiint \mathbf{u}P(c,\mathbf{u},\mathbf{x},t)d\mathbf{u}\right]dc,\end{aligned} \tag{6.44}$$

where $\varepsilon \ll 1$ is a small number. Because the probabilities $P_u(\mathbf{u},t,\mathbf{x})$ and $P_b(\mathbf{u},t,\mathbf{x})$ are unknown, the conditioned velocities $\bar{\mathbf{u}}_u$ and $\bar{\mathbf{u}}_b$ are also unknown and require modeling.

Equation (6.35) is widely used as a state equation in RANS simulations of premixed turbulent flames. Equations (6.39)–(6.43) are widely used when interpreting experimental data and discussing the influence of combustion on turbulence, as will be demonstrated in the next section. In the rest of the present chapter, all the BML equations are considered to be valid and $O(\gamma)$-terms will be neglected if the opposite is not stated.

The same equations can be derived within the framework of the two-fluid approximation. In this case, the conditioned velocities are defined as follows

$$(1-\bar{c})\tilde{\mathbf{u}}_u = \overline{(1-c)\mathbf{u}}, \qquad \bar{c}\tilde{\mathbf{u}}_b = \overline{c\mathbf{u}}. \tag{6.45}$$

If the state of a mixture in a flame is characterized with a single combustion progress variable, then, within the RANS framework, the adiabatic and iso-baric combustion process is modeled using a single specific transport Eq. (6.27) in addition to the Favre-averaged continuity and Navier–Stokes equations, i.e., Eqs. (6.15) and (6.16), respectively. To close the problem, all terms on the RHS of Eq. (6.27) and the Reynolds stresses $\overline{\rho u_i'' u_j''}$ in Eq. (6.16) should be modeled.

The first, molecular transport, term on the RHS of Eq. (6.27) is often neglected when compared to other terms if turbulent Reynolds number is sufficiently large. Modeling of the turbulent scalar flux $\overline{\rho \mathbf{u}'' c''}$ and the mean reaction rate $\overline{\dot{\omega}_c}$ is addressed in the next two Sects. 6.3.1 and 6.3.2, respectively.

To conclude the present section, it is worth noting that the approximation of a single-step chemistry appears to be the best tool (i) for qualitatively discussing most important local effects associated with flame–turbulence interaction and (ii) for developing closure relations for $\overline{\rho \mathbf{u}'' c''}$ and, especially, $\overline{\dot{\omega}_c}$. However, when applying these closure relations in CFD research, it is better to invoke two-fluid or BML approach, because it offers an opportunity to use values of $\rho_b$, $T_b$, and species mass fractions $Y_{k,b}$, which are calculated for a mixture of $H_2O$, $CO_2$, CO, $O_2$, $H_2$, OH, O, H, etc.

### 6.3.2 *Effects of Combustion on Turbulence and Model Challenges*

The problems of modeling the flux $\overline{\rho \mathbf{u}'' c''}$ and the Reynolds stresses $\overline{\rho u_i'' u_j''}$ are not specific to turbulent combustion and were thoroughly investigated in studies of (i) turbulent mixing in constant-density flows and (ii) turbulent flows, respectively. However, due to significant density variations localized to thin zones, combustion generates variety of new effects and makes the problem much more difficult, as briefly discussed in the present section. The reader interested in a more detailed discussion of these effects and approaches to modeling them is referred to recent review papers (Lipatnikov and Chomiak 2010; Sabelnikov and Lipatnikov 2017) and monograph (Lipatnikov 2012).

#### 6.3.2.1 Transport Equations for Second Moments

At first glance, the problem of modeling the second moments $\overline{\rho u_i'' c''}$ and $\overline{\rho u_i'' u_j''}$ of turbulent fields $\mathbf{u}(\mathbf{x}, t)$ and $c(\mathbf{x}, t)$ might be solved by deriving appropriate transport equations, as such a derivation is straightforward. For instance, let us, first, (i) use the continuity Eq. (6.2) to move $\rho$ and $\rho u_j$ outside the time and spatial derivatives on the Left Hand Side (LHS) of Eq. (6.3) or (6.23), (ii) multiply the two equations with $c$ and $u_i$, respectively, and sum them, (iii) use the continuity Eq. (6.2) to move $\rho$ and $\rho u_j$ inside the time and spatial derivatives on the LHS of the obtained equation. Then, we arrive at

$$\frac{\partial}{\partial t}\left(\rho u_i c\right) + \frac{\partial}{\partial x_j}\left(\rho u_i u_j c\right) = c\frac{\partial \tau_{ij}}{\partial x_j} - c\frac{\partial p}{\partial x_i} + u_i \frac{\partial}{\partial x_j}\left(\rho D \frac{\partial c}{\partial x_j}\right) + u_i \dot{\omega}_c. \tag{6.46}$$

Second, application of a similar algorithm to the Favre-averaged Eqs. (6.16) and (6.27) results in

$$\begin{aligned}\frac{\partial}{\partial t}\left(\bar{\rho}\tilde{u}_i\tilde{c}\right) + \frac{\partial}{\partial x_j}\left(\bar{\rho}\tilde{u}_i\tilde{u}_j\tilde{c}\right) = &-\tilde{c}\frac{\partial}{\partial x_j}\overline{\rho u_i'' u_j''} - \tilde{u}_i \frac{\partial}{\partial x_j}\overline{\rho u_j'' c''} \\ &+\tilde{u}_i \frac{\partial}{\partial x_j}\left(\overline{\rho D \frac{\partial c}{\partial x_j}}\right) + \tilde{c}\frac{\partial \bar{\tau}_{ij}}{\partial x_j} - \tilde{c}\frac{\partial \bar{p}}{\partial x_i} + \tilde{u}_i \overline{\dot{\omega}_c}.\end{aligned} \tag{6.47}$$

Third, the Favre-averaged Eq. (6.46) reads

$$\begin{aligned}&\frac{\partial}{\partial t}\left(\bar{\rho}\tilde{u}_i\tilde{c}\right) + \frac{\partial}{\partial t}\overline{\rho u_i'' c''} + \frac{\partial}{\partial x_j}\left(\bar{\rho}\tilde{u}_i\tilde{u}_j\tilde{c}\right) + \frac{\partial}{\partial x_j}\left(\tilde{u}_j\overline{\rho u_i'' c''}\right) \\ &= -\frac{\partial}{\partial x_j}\left(\tilde{u}_i\overline{\rho u_j'' c''} + \tilde{c}\overline{\rho u_i'' u_j''}\right) - \frac{\partial}{\partial x_j}\overline{\rho u_i'' u_j'' c''} + \tilde{c}\frac{\partial \bar{\tau}_{ij}}{\partial x_j} + \overline{c''\frac{\partial \tau_{ij}}{\partial x_j}} \\ &-\tilde{c}\frac{\partial \bar{p}}{\partial x_i} - \overline{c''\frac{\partial p}{\partial x_i}} + \tilde{u}_i \frac{\partial}{\partial x_j}\left(\overline{\rho D \frac{\partial c}{\partial x_j}}\right) + \overline{u_i''\frac{\partial}{\partial x_j}\left(\rho D \frac{\partial c}{\partial x_j}\right)} + \tilde{u}_i\overline{\dot{\omega}_c} + \overline{u_i''\dot{\omega}_c},\end{aligned} \tag{6.48}$$

because $\overline{\rho a b c} = \overline{\rho(\tilde{a}+a'')(\tilde{b}+b'')(\tilde{c}+c'')} = \bar{\rho}\tilde{a}\tilde{b}\tilde{c} + \overline{\rho a''}\tilde{b}\tilde{c} + \overline{\rho b''}\tilde{a}\tilde{c} + \overline{\rho c''}\tilde{a}\tilde{b} + \overline{\rho a'' b''}\tilde{c} + \overline{\rho a'' c''}\tilde{b} + \overline{\rho b'' c''}\tilde{a} + \overline{\rho a'' b'' c''} = \bar{\rho}\tilde{a}\tilde{b}\tilde{c} + \overline{\rho a'' b''}\tilde{c} + \overline{\rho a'' c''}\tilde{b} + \overline{\rho b'' c''}\tilde{a} + \overline{\rho a'' b'' c''}$ for arbitrary quantities $a$, $b$, and $c$.

Finally, subtraction of Eq. (6.47) from Eq. (6.48) yields

$$\begin{aligned}\frac{\partial}{\partial t}\overline{\rho u_i'' c''} + \frac{\partial}{\partial x_j}\left(\tilde{u}_j\overline{\rho u_i'' c''}\right) = &\underbrace{-\overline{\rho u_i'' u_j''}\frac{\partial \tilde{c}}{\partial x_j} - \overline{\rho u_j'' c''}\frac{\partial \tilde{u}_i}{\partial x_j}}_{\text{i}} \underbrace{-\frac{\partial}{\partial x_j}\overline{\rho u_i'' u_j'' c''}}_{\text{ii}} \\ &\underbrace{+\overline{c''\frac{\partial \tau_{ij}}{\partial x_j}}}_{\text{iii}} \underbrace{+\overline{u_i''\frac{\partial}{\partial x_j}\left(\rho D \frac{\partial c}{\partial x_j}\right)}}_{\text{iv}} \underbrace{-\overline{c''\frac{\partial p'}{\partial x_i}}}_{\text{v}} \underbrace{-\overline{c''}\frac{\partial \bar{p}}{\partial x_i}}_{\text{vi}} \underbrace{+\overline{u_i''\dot{\omega}_c}}_{\text{vii}}.\end{aligned} \tag{6.49}$$

Using a similar method, the following transport equation for the Reynolds stresses

$$\frac{\partial}{\partial t}\overline{\rho u_i'' u_j''} + \frac{\partial}{\partial x_l}\left(\tilde{u}_l \overline{\rho u_i'' u_j''}\right) = \underbrace{-\overline{\rho u_j'' u_l''}\frac{\partial \tilde{u}_i}{\partial x_l} - \overline{\rho u_i'' u_l''}\frac{\partial \tilde{u}_j}{\partial x_l}}_{\text{I}} \tag{6.50}$$

$$\underbrace{-\frac{\partial}{\partial x_l}\overline{\rho u_i'' u_j'' u_l''}}_{\text{II}} \underbrace{+\overline{u_j''\frac{\partial \tau_{il}}{\partial x_l}} + \overline{u_i''\frac{\partial \tau_{jl}}{\partial x_l}}}_{\text{III}} \underbrace{-\overline{u_j''\frac{\partial p'}{\partial x_i}} - \overline{u_i''\frac{\partial p'}{\partial x_j}}}_{\text{IV}} \underbrace{-\overline{u_j''}\frac{\partial \bar{p}}{\partial x_i} - \overline{u_i''}\frac{\partial \bar{p}}{\partial x_j}}_{\text{V}}$$

can be derived.

The transport Eqs. (6.49) and (6.50) do not resolve the problem of closing the turbulent scalar flux $\overline{\rho u_i'' c''}$ and the Reynolds stresses $\overline{\rho u_i'' u_j''}$, because these transport equations involve a number of new unclosed terms, i.e., terms (ii)–(vii) on the RHS of Eq. (6.49) and terms (II)–(V) on the RHS of Eq. (6.50). It is worth stressing that some of these unclosed terms are specific to turbulent combustion. Indeed, application of the two transport equations to a constant-density non-reacting flow results in

$$\frac{\partial}{\partial t}\overline{u_i' c'} + \frac{\partial}{\partial x_j}\left(\overline{u_j u_i' c'}\right) = \underbrace{-\overline{u_i' u_j'}\frac{\partial \bar{c}}{\partial x_j} - \overline{u_j' c'}\frac{\partial \bar{u}_i}{\partial x_j}}_{\text{i}'} \underbrace{-\frac{\partial}{\partial x_j}\overline{u_i' u_j' c'}}_{\text{ii}'}$$

$$\underbrace{+\nu\overline{c'\frac{\partial^2 u_i'}{\partial x_j^2}}}_{\text{iii}'} \underbrace{+D\overline{u_i'\frac{\partial^2 c'}{\partial x_j^2}}}_{\text{iv}'} \underbrace{-\frac{1}{\rho}\overline{c'\frac{\partial p'}{\partial x_i}}}_{\text{v}'} \tag{6.51}$$

and

$$\frac{\partial}{\partial t}\overline{u_i' u_j'} + \frac{\partial}{\partial x_l}\left(\overline{u_l u_i' u_j'}\right) = \underbrace{-\overline{u_j' u_l'}\frac{\partial \bar{u}_i}{\partial x_l} - \overline{u_i' u_l'}\frac{\partial \bar{u}_j}{\partial x_l}}_{\text{I}'}$$

$$\underbrace{-\frac{\partial}{\partial x_l}\overline{u_i' u_j' u_l'}}_{\text{II}'} \underbrace{+\nu\left(\overline{u_j'\frac{\partial^2 u_i'}{\partial x_l^2}} + \overline{u_i'\frac{\partial^2 u_j'}{\partial x_l^2}}\right)}_{\text{III}'} \underbrace{-\frac{1}{\rho}\left(\overline{u_j'\frac{\partial p'}{\partial x_i}} - \overline{u_i'\frac{\partial p'}{\partial x_j}}\right)}_{\text{IV}'}. \tag{6.52}$$

Equation (6.51) does not contain counterparts of terms (vi) and (vii) on the RHS of Eq. (6.49), with an important role played by these terms in premixed turbulent flames being documented in DNS studies reviewed elsewhere (Lipatnikov and Chomiak 2010). Similarly, Eq. (6.52) does not contain a counterpart of term V on the RHS of Eq. (6.50), with this term also playing an important role in premixed turbulent flames (Lipatnikov and Chomiak 2010).

Because transport equations for the considered second moments are substantially different in the cases of a non-reacting constant-density turbulent flow and a premixed turbulent flame, we could expect that closure relations developed for $\overline{u_i' c'}$ and $\overline{u_i' u_j'}$ may be inappropriate in the latter case.

#### 6.3.2.2 Countergradient Turbulent Transport

For instance, when modeling turbulent mixing in constant-density flows, the following gradient diffusion closure relation

$$\overline{\mathbf{u}'' c''} = -D_t \nabla \tilde{c} \tag{6.53}$$

is widely used. Here, $D_t > 0$ is the turbulent diffusivity given by an invoked model of turbulence and it is worth remembering that $\bar{q} = \tilde{q}$ and $q'' = q'$ in the case of a constant density. However, as well documented in various experiments reviewed elsewhere (Bray 1995; Lipatnikov and Chomiak 2010; Sabelnikov and Lipatnikov 2017), the scalar product of $\overline{\mathbf{u}'' c''} \cdot \nabla \tilde{c}$ may be positive in premixed flames, contrary to Eq. (6.53). This phenomenon is known as countergradient turbulent transport. It was predicted by Clavin and Williams (1979) and Libby and Bray (1981) and was first documented in experiments by Moss (1980) and by Yanagi and Mimura (1981).

The simplest explanation of the countergradient turbulent transport in premixed flames is as follows. Equation (6.41) shows that $(\bar{\mathbf{u}}_b - \bar{\mathbf{u}}_u) \cdot \nabla \tilde{c} > 0$ in the case of the countergradient turbulent transport. In particular, $\bar{u}_b > \bar{u}_u$ within a statistically planar 1D turbulent flame brush[2] sketched in Fig. 6.1. This difference in $\bar{u}_b$ and $\bar{u}_u$ may stem from the following two physical mechanisms.

First, the mean pressure gradient $\nabla \bar{p}$ induced within the mean flame brush due to thermal expansion accelerates lighter products stronger than denser unburned gas (Libby and Bray 1981; Scurlock and Grover 1953), because $\partial \mathbf{u}/\partial t \propto \rho^{-1} \nabla p$ due to Navier–Stokes equations. For instance, the axial velocity in point A′ in Fig. 6.1 is larger than the axial velocity in point A or B, because the burned gas is significantly accelerated by the mean pressure gradient when moving from point A to A′, whereas such an acceleration is weak in the unburned gas and even negligible if $\rho_u \gg \rho_b$

Second, due to thermal expansion, the normal gas velocity increases from unburned to burned edges of a laminar premixed flame (Zel'dovich et al. 1985) and similar jumps in $|\mathbf{u} \cdot \mathbf{n}|$ occur locally at flame fronts in turbulent flows, e.g., in point A or B in Fig. 6.1. Here, $\mathbf{n} = -\nabla c/|\nabla c|$ is a unit vector that is locally normal to the flamelet and points to the unburned gas.

In a turbulent flow, the two aforementioned mechanisms associated with thermal expansion are counteracted by velocity fluctuations, which yield turbulent diffusion in constant-density flows. Accordingly, depending on conditions, both the counter-

[2]Premixed turbulent flame brush is a spatial volume where the probabilities of finding $c = 0$ and $c = 1$ are both less than unity.

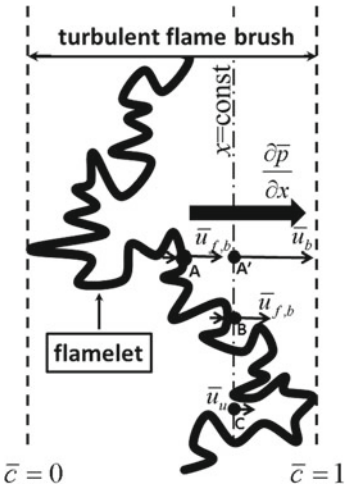


**Fig. 6.1** Preferential acceleration of burned gas due to thermal expansion

gradient turbulent transport and gradient diffusion associated with $\overline{\rho \mathbf{u}'' c''} \cdot \nabla \tilde{c} < 0$ can occur in premixed turbulent flames. It is widely accepted that the countergradient turbulent transport dominates if the Bray number (Bray 1995) defined as follows:

$$N_B = \frac{\tau S_L}{u'} \tag{6.54}$$

is substantially larger than unity, whereas the gradient diffusion is often associated with a low $N_B$. It is worth stressing, however, that the sign of $\overline{\rho \mathbf{u}'' c''} \cdot \nabla \tilde{c}$ depends also on other flow and mixture characteristics, as discussed in detail elsewhere (Lipatnikov and Chomiak 2010). For instance, the sign of the flux $\overline{\rho \mathbf{u}'' c''}$ may change its direction during premixed turbulent flame development (Lipatnikov 2011b), but the Bray number does not involve flame-development time.

Over the first two decades, since the discovery of the countergradient turbulent transport in premixed flames (Clavin and Williams 1979; Libby and Bray 1981; Moss 1980; Yanagi and Mimura 1981), the sole approach to modeling this phenomenon within the RANS framework consisted in developing closure relations for various terms in Eq. (6.49). However, as discussed in detail elsewhere (Lipatnikov and Chomiak 2010), such efforts have not yet yielded a model whose predictive capabilities were well documented against a representative set of experimental or DNS data obtained from substantially different flames under substantially different conditions.

Accordingly, over the past years, alternative approaches were developed by placing the focus of modeling on the conditioned velocities $\tilde{\mathbf{u}}_u$ and $\tilde{\mathbf{u}}_b$. The reader interested in a review of such models is referred to (Sabelnikov and Lipatnikov 2017). At the moment, there is no model that is widely recognized to be able to predict the flux $\overline{\rho \mathbf{u}'' c''}$ under substantially different conditions, including transition from $\overline{\rho \mathbf{u}'' c''} \cdot \nabla \tilde{c} > 0$ to $\overline{\rho \mathbf{u}'' c''} \cdot \nabla \tilde{c} < 0$. Nevertheless, certain progress in validation of

recently proposed models was made. For instance, the following simple closure relation (Lipatnikov et al. 2015c; Sabelnikov and Lipatnikov 2011)

$$(1-\bar{c})\nabla\cdot\bar{\mathbf{u}}_u \approx (-0.18+0.35\sigma)\frac{(1-\bar{c})^{1/2}}{(1+u'/S_L)^{1/2}}\frac{u'}{S_L}\overline{\dot{\omega}_c} \tag{6.55}$$

was validated against experimental and DNS data associated with the countergradient turbulent transport in premixed flames, see Figs. 6.2, 6.3 and 6.4, respectively.

Numerical results reported in Figs. 6.2, 6.3 and 6.4 were obtained by simulating flames described by statistically 1D transport equations. In such a case, a single scalar Eq. (6.55) allows us to evaluate a single conditioned velocity $\bar{u}_u$, followed by calculation of a single component of the turbulent flux vector $\overline{\rho u'' c''}$ using Eq. (6.41). However, a single scalar Eq. (6.55) is not sufficient to obtain two or three components of the conditioned vector $\bar{\mathbf{u}}_u$ in a statistically 2D or 3D case, respec-

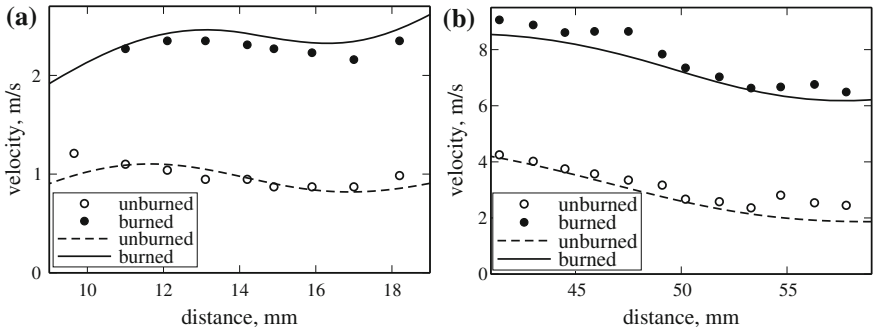


**Fig. 6.2** Velocities conditioned to unburned (open symbols or dashed lines) and burned (filled symbols or solid lines) gases. Circles show experimental data obtained by **a** Cho et al. (1988) and **b** Cheng and Shepherd (1991) from impinging-jet flames. Solid lines show results computed by Lipatnikov et al. (2015c) using Eq. (6.55)

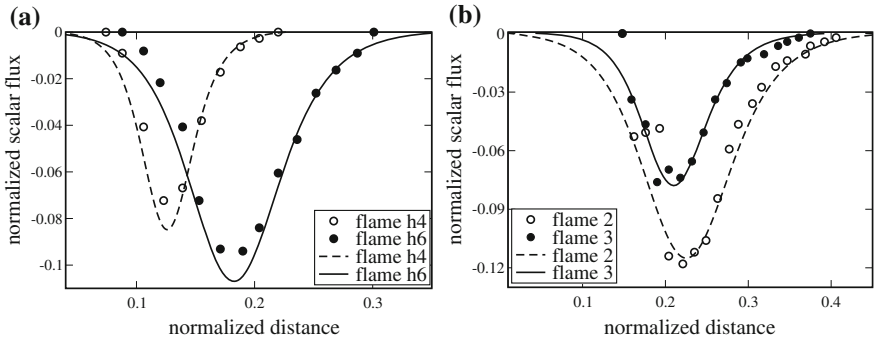


**Fig. 6.3** Turbulent scalar fluxes measured (symbols) by **a** Li et al. (1994) and **b** Stevens et al. (1998) and computed (lines) by Lipatnikov et al. (2015c) using Eqs. (6.41) and (6.55)

tively. In recent 2D RANS simulations (Yasari and Lipatnikov 2015) of open conical rim-stabilized (Bunsen) methane–air flames that were experimentally investigated by Frank et al. (1999) and Pfadler et al. (2008), the problem was resolved by invoking the gradient diffusion closure of the tangential (to the mean flame brush) component of the flux vector $\overline{\rho \mathbf{u}'' c''}$, i.e., the tangential flux vanished in that model. In line with the former measurements (Frank et al. 1999), the simulations (Yasari and Lipatnikov 2015) yielded reduction of the magnitude of the countergradient flux followed by transition to gradient diffusion at $\Phi = 0.7$ when $\Phi$ was decreased from $\Phi = 1$ to 0.6. In line with the latter measurements (Pfadler et al. 2008), the simulations (Yasari and Lipatnikov 2015) yielded the countergradient flux in the radial (almost normal to the mean flame brush) direction in all studied flames, with the magnitude of the flux being weakly decreased with increasing the inlet mass flow rate, but being significantly increased by the equivalence ratio in the lean flames.

Thus, the aforementioned RANS tests of Eq. (6.55) yielded encouraging results, but further studies aimed at validating and applying this simple model are definitely required.

#### 6.3.2.3 Flame-Generated Turbulence

The problem of flame-generated turbulence was raised by Karlovitz (1951) and by Scurlock and Grover (1953) and was studied in many subsequent papers reviewed elsewhere (Lipatnikov and Chomiak 2010). This problem is commonly considered to be of paramount importance, because turbulence eventually generated due to thermal expansion in a premixed flame was hypothesized to significantly increase the burning rate (Karlovitz et al. 1951).

In principle, both countergradient turbulent flux and flame-generated turbulence are caused by the same physical mechanisms. First, the jump in the locally normal velocity at a flamelet contributes not only to an increase in $|\tilde{\mathbf{u}}_b|$ when compared to

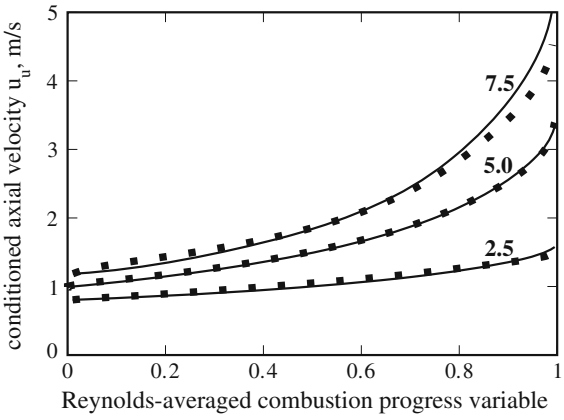


**Fig. 6.4** Turbulent scalar fluxes obtained by processing DNS data (symbols) and computed (lines) using Eq. (6.55) (Lipatnikov et al. 2015c). Three different flames characterized by three different density ratios specified near lines and symbols

$|\bar{\mathbf{u}}_u|$, as discussed in the previous section, see points A and B in Fig. 6.1, but also to an increase in the magnitude of velocity fluctuations due to fluctuations in the direction of the normal vector $\mathbf{n}$ and, hence, in the direction of the local velocity jump. This physical mechanism was highlighted by Karlovitz et al. (1951).

Second, preferential acceleration of the burned gas by combustion-induced pressure gradient not only contributes to an increase in $|\bar{\mathbf{u}}_b|$ when compared to $|\bar{\mathbf{u}}_u|$, as discussed in the previous section, but also generates a shear flow behind flamelets, because some product volumes, e.g., see point A′ in Fig. 6.1, are accelerated during a longer time interval when compared to other product volumes, see point B. Subsequently, the shear flow generates turbulence. This physical mechanism was highlighted by Scurlock and Grover (1953).

Although both the countergradient turbulent transport and flame-generated turbulence are governed by basically the same mechanisms, as discussed above, models of the latter phenomenon have yet been developed substantially worse when compared to models of the former phenomenon. In particular, within the RANS framework, flame-generated turbulence is still addressed mainly using Eq. (6.50) and developing closure relations for various terms on the RHS. However, such efforts have not yet yielded a widely recognized model whose predictive capabilities were well documented against a representative set of experimental or DNS data obtained from substantially different flames under substantially different conditions. Accordingly, in RANS simulations of premixed turbulent flames, the problem of flame-generated turbulence is often ignored by invoking a turbulence model, e.g., the $k$-$\varepsilon$ one (Launder and Spalding 1972), that was developed and validated in the non-reacting constant-density case.

#### 6.3.2.4 Can We Properly Characterize Turbulence in a Flame?

It is also worth stressing that appropriateness of the Reynolds stresses $\overline{\rho u_i'' u_j''}$ for characterizing turbulence in premixed flames may be put into question (Lipatnikov 2009a, 2011a; Lipatnikov and Chomiak 2010; Sabelnikov and Lipatnikov 2017). For instance, Eq. (6.43) clearly shows that $\overline{\rho u_i'' u_j''}$ is controlled not only by the Reynolds stresses $(\overline{u_i' u_j'})_u$ and $(\overline{u_i' u_j'})_b$ conditioned to unburned and burned mixtures, respectively, but also by the unburned–burned intermittency term, which involves differences in velocities conditioned to the unburned and burned mixtures, see the last term on the RHS. If this difference is on the order of $\tau S_L$, then, the last term on the RHS scales as $(\tau S_L)^2$ and can be much larger than two other terms in the case of a weak turbulence, i.e., $u'/S_L = O(1)$. However, this term is not associated with turbulence, because the local normal velocity jump at a flamelet is controlled by the local combustion-induced pressure gradient and, therefore, does not change the local vorticity[3] $\nabla \times \mathbf{u}$. On the contrary, turbulence is considered to be inherently rotational

[3]If the curl operator is applied to the Navier–Stokes equations, then, the pressure gradient term vanishes, because $\nabla \times \nabla q \equiv 0$ for any scalar quantity $q$.

3D flow. Therefore, the irrotational velocity jump and the local turbulence generation appear to be two fundamentally different phenomena, which should be characterized by different quantities.

Accordingly, the conditioned Reynolds stresses $(\overline{u_i'u_j'})_u$ and $(\overline{u_i'u_j'})_b$ are often considered to be fundamentally more proper characteristics of turbulence in the unburned and burned gases, respectively, within a premixed flame brush. For instance, the physical mechanism highlighted by Scurlock and Grover (1953), i.e., generation of turbulence by shear caused by the preferential acceleration of light products by the combustion-induced bulk pressure gradient, is clearly associated with generation of turbulence in the burned gas. However, a physical mechanism of eventual influence of turbulence generated behind flamelets on the flamelet propagation into the unburned reactants has not yet been revealed.

Local variations in turbulence characteristics just upstream of flamelets appear to be of much more importance when discussing eventual self-acceleration of premixed flames due to combustion-induced turbulence. From this perspective, the Reynolds stresses $(\overline{u_i'u_j'})_u$ conditioned to the unburned mixture appear to be the best turbulence characteristics within a premixed flame brush at first glance and such a standpoint is shared by many experts. Nevertheless, this standpoint can be disputed. Due to random motion of an interface that separates two fluids, a statistical sub-ensemble over that a conditional average is taken depends on $\mathbf{x}$ and $t$, as is well known in the theory of intermittent flows (Kuznetsov and Sabelnikov 1990; Libby 1975; Townsend 1976). Consequently, the conditioned second moments differ from their mean counterparts even in the case of self-propagation of a passive interface in a constant-density flow, whereas it is the mean moments that characterize turbulence that is not affected by the interface propagation.

For combustion applications, this feature of conditionally averaged second moments follows straightforwardly from Eq. (6.43), which shows that $(\overline{u_i'u_j'})_u$ differs from $\overline{u_i'u_j'}$ even in the constant-density case, but it is the latter quantity that properly characterizes turbulence in such a case. The same feature of conditionally averaged second moments was also demonstrated by analyzing simple model problems (Lipatnikov 2009a, 2011a) and was recently shown in a 3D DNS study of self-propagation of an infinitely thin and dynamically passive interface in constant-density turbulence (Yu et al. 2014, 2015). The DNS also indicated that quantities controlled by velocity gradients were significantly less sensitive to averaging method. In particular, the mean and conditioned total strains $S^2 = S_{ij}S_{ij}$ or enstrophies $\omega^2 = (\nabla \times \mathbf{u})^2$ were almost equal to one another in all simulated cases, thus, implying that $(\overline{S^2})_u$ or $(\overline{\omega^2})_u$ is a proper characteristic of turbulence in reactants at least in the case of a constant density. Here, $S_{ij} = (\partial u_i/\partial x_j + \partial u_j/\partial x_i)/2$ is the rate-of-strain tensor.

All in all, the problem of characterizing turbulence within a premixed turbulent flame brush strongly requires further research. It is worth noting that this unresolved fundamental problem reduces the importance of another unresolved problem, i.e., modeling of $\overline{\rho u_i'' u_j''}$ and $(\overline{u_i'u_j'})_u$ or $(\overline{u_i'u_j'})_b$ in premixed turbulent flames. Indeed, if

neither of these second moments properly characterizes flame-turbulence interaction, then, modeling of these second moments appear to be of secondary importance.

#### 6.3.2.5 Flow Perturbations Upstream of a Flame. Hydrodynamic Instability

As already noted, perturbations of the incoming flow of unburned reactants appear to be required in order for thermal expansion effects cause self-acceleration of the flame. Such a kind of flow perturbations is well known in the theory of laminar combustion and causes the hydrodynamic instability of laminar premixed flames, which was theoretically discovered by Darrieus (1938) and Landau (1944). In honor of these two scientists, the instability is often called the DL instability.

As discussed in many combustion textbooks (Law 2006; Lipatnikov 2012; Poinsot and Veynante 2005; Williams 1985; Zel'dovich et al. 1985), the physical mechanism of the DL instability is as follows. Due to flow acceleration in the direction normal to a laminar flame, the flow velocity vector changes its direction when crossing the flame, with the magnitude of $\mathbf{u} \cdot \mathbf{n}/|\mathbf{u}|$ being larger on the burned side of the flame (or $|\mathbf{u} \cdot \mathbf{n}|/|\mathbf{u}| = 1$ on both sides of the flame if the vectors $\mathbf{u}$ and $\mathbf{n}$ are parallel to one another). Such a change in the flow velocity vector direction is illustrated in insert associated with point B in Fig. 6.5. Accordingly, if the flame surface is subject to infinitesimal perturbations, see solid line in Fig. 6.5, then, the flame induces divergence (convergence) of the unburned (burned) mixture flow upstream (downstream) of convex (toward the unburned gas, see arc AB) elements of the flame surface, see fluid tubes bounded by flow lines A′A and B′B (AA″ and BB″, respectively). Consequently, the flow velocity of unburned gas at the convex flame surface decreases, whereas the flame speed $S_L$ is assumed to be constant within the framework of the DL theory. Similarly, the flame induces convergence (divergence) of the unburned (burned) mixture flow upstream (downstream) of concave elements (arc BC) of the flame surface, see fluid tubes bounded by flow lines C′C and B′B (CC″ and BB″, respectively), and the flow velocity of unburned gas at the concave flame surface increases. As a result, convex (arc AB) and concave (arc BC) bulges are characterized by $|\mathbf{u}_u \cdot \mathbf{n}| < S_L$ and $|\mathbf{u}_u \cdot \mathbf{n}| > S_L$, respectively. Therefore, the bulges grow, the amplitude of the flame surface perturbation increases, and the flame becomes unstable. This instability is the classical example of self-acceleration of a flame due to perturbations of the incoming flow of unburned reactants, caused by thermal expansion in the flame.

Flamelets in a turbulent flow may also be subject to such a local DL instability, which results in increasing flamelet surface area and, hence, turbulent burning rate. However, such effects appear to be of substantial importance only in weak turbulence, i.e., if a ratio of $u'/S_L = O(1)$ (Boughanem and Trouvé 1998; Chaudhuri et al. 2011; Fogla et al. 2017; Lipatnikov and Chomiak 2005c). Nevertheless, the governing physical mechanism of the DL instability, i.e., acceleration of unburned mixture flow due to combustion-induced pressure gradient, may manifest itself in other phenomena, e.g., the growth of the so-called unburned mixture fingers that deeply

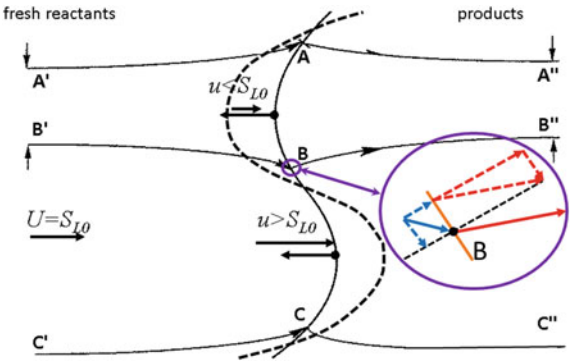


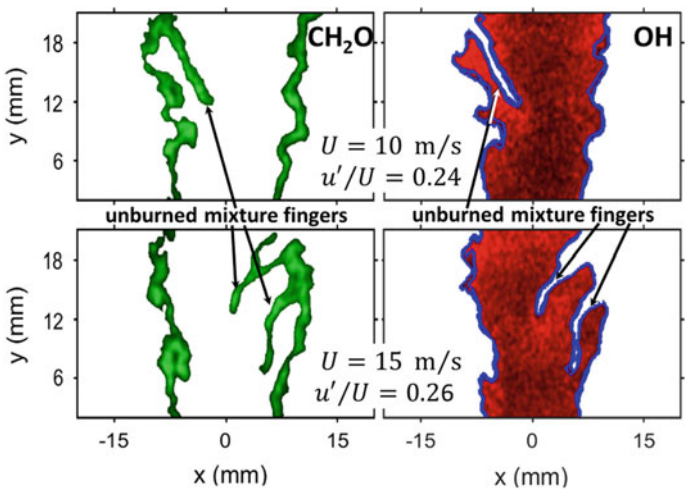


**Fig. 6.5** Physical mechanism of the DL instability

**Fig. 6.6** Unburned mixture fingers in bluff body stabilized conical lean premixed turbulent flames. Adapted from the paper by Chowdhury and Cetegen (2017)

intrude into combustion products (Lipatnikov et al. 2015b). A recent image of such fingers is shown in Fig. 6.6. The latter manifestation of the DL mechanism differs from the hydrodynamic instability of laminar flames, caused by the same mechanism, because the magnitude of pressure gradient within a premixed turbulent flame brush may be much larger than the magnitude of pressure gradient in unburned gas in the vicinity of a weakly wrinkled laminar premixed flame.

Moreover, pressure perturbations induced due to thermal expansion in flamelets may rapidly propagate upstream of the flame brush and change the incoming velocity field (Sabelnikov and Lipatnikov 2017). Such effects require thorough investigation.

#### 6.3.2.6 Summary

Modeling of the influence of premixed combustion on turbulence and turbulent transport is the weakest point of the contemporary theory of turbulent combustion. While certain promising approaches to modeling turbulent transport in premixed flames were recently put forward, other fundamental issues such as

- selection of proper turbulence characteristics in flames,
- modeling of these turbulence characteristics, and
- eventual self-acceleration of premixed flames due to combustion-induced perturbations of the incoming flow of unburned reactants

have not yet been resolved even in a first approximation.

In applied CFD research into turbulent combustion, these fundamental issues are commonly disregarded and turbulence is modeled invoking methods developed and validated in studies on non-reacting constant-density flows.

While such a practical solution appears to be justified unless the aforementioned issues are resolved, it is still unclear why results of such applied simulations agreed with experimental data in a number of studies.

One possible answer consists in (i) highlighting a crucial role played by the leading edge of a premixed turbulent flame brush in its propagation and (ii) assuming that effects of combustion on turbulence are weak at the leading edge. However, this subject is beyond the scope of the present chapter and the interested reader is referred to a review paper (Lipatnikov and Chomiak 2005c), a monograph (Lipatnikov 2012), and recent papers (Kha et al. 2016; Kim 2017; Sabelnikov and Lipatnikov 2013, 2015; Venkateswaran et al. 2015).

### 6.3.3 *Effects of Turbulence on Combustion: Problems, Physical Mechanisms, and Models*

A major challenge of premixed turbulent combustion modeling within the RANS framework stems from (i) highly nonlinear dependencies of the rates of reactions that control heat release on the temperature and (ii) large magnitude of the temperature fluctuations in a turbulent flow. Accordingly, $\dot{\omega}_c$ depends on $c$ in a highly nonlinear manner and is subject to large fluctuations in $c$, from zero to unity and back.

To illustrate the problem, let us compare $\overline{\exp\left(-\Theta/T\right)}$ and $\exp\left(-\Theta/\overline{T}\right)$ in a point where the probabilities of finding unburned and burned mixtures are equal to 0.5, i.e., the probability of finding the intermediate temperatures is assumed to be negligible in the considered example. In the case of $T_u = 300$ K, $T_b = 2200$ K, and $\Theta = 20000K$, we have $\overline{T} = 1250$ K and $\exp\left(-\Theta/\overline{T}\right) = 1.1 \times 10^{-7}$, whereas $\overline{\exp\left(-\Theta/T\right)} \approx 0.5\overline{\exp\left(-\Theta/T_b\right)} = 5.6 \times 10^{-5}$, i.e., the former exponential term is lower than the latter term by a factor os 500!

Obviously, such a huge difference cannot be modeled by expanding $\exp(-\Theta/T)$ into the Taylor series with respect to $T'/\overline{T}$, followed by averaging, e.g.,

$$\overline{\exp\left(-\frac{\Theta}{T}\right)} = \overline{\exp\left\{-\frac{\Theta}{\overline{T}}\left[1-\frac{T'}{\overline{T}}+\left(\frac{T'}{\overline{T}}\right)^2-\left(\frac{T'}{\overline{T}}\right)^3+\left(\frac{T'}{\overline{T}}\right)^4\right\}+\cdots\right]}$$
$$= \exp\left(-\frac{\Theta}{\overline{T}}\right)\left[1+\frac{3}{2}\overline{\left(\frac{T'}{\overline{T}}\right)^2}-\frac{13}{6}\overline{\left(\frac{T'}{\overline{T}}\right)^3}+\frac{73}{22}\overline{\left(\frac{T'}{\overline{T}}\right)^4}+\ldots\right]. \quad (6.56)$$

In the considered example ($\bar{c}=0.5$, $T_u=300$ K, $T_b=2200$ K, $\overline{T}=1250$ K, and $\Theta=20000K$), the odd moments $\overline{(T'/\overline{T})^{2n+1}}$ vanish, whereas the even moments $\overline{(T'/\overline{T})^{2n}}$ are equal to $[(T_b-T_u)/2\overline{T}]^{2n}=0.76^{2n}$. Here, $n\geq 1$ is an integer number. Consequently, the use of the first-order terms in the above Taylor series does not allow us to increase $\overline{\exp(-\Theta/T)}$ by a required factor of 500 when compared to $\exp\left(-\Theta/\overline{T}\right)$. Thus, standard perturbation methods cannot be used to predict the influence of strong turbulent fluctuations in the temperature (or the combustion progress variable $c$) on reaction rates that depend on $T$ (or $c$) in a highly nonlinear manner, e.g. $\dot{\omega}_c(c)$. To resolve the problem, RANS models of premixed turbulent combustion are commonly developed by highlighting a few of many physical mechanisms of flame–turbulence interaction.

#### 6.3.3.1 Physical Mechanisms

When discussing physical mechanisms of the influence of turbulence on premixed combustion, there are several levels of simplifications, which are illustrated in Fig. 6.7.

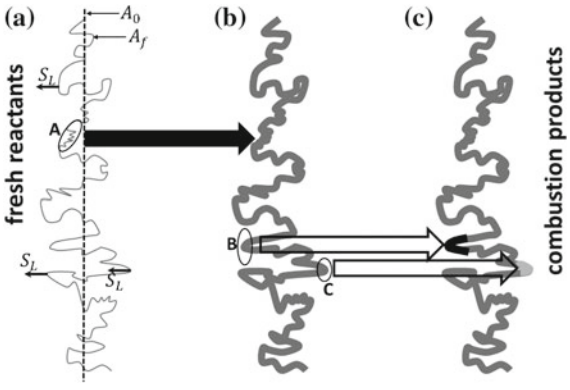


**Fig. 6.7** Various effects associated with the influence of turbulence on premixed combustion

At the first, simplest level, the influence of turbulence on premixed combustion is solely reduced to wrinkling an infinitely thin flame front by turbulent eddies, see Fig. 6.7a, with the front speed with respect to the unburned gas being assumed to be constant and equal to $S_L$. The first models of that kind were put forward by Damköhler (1940) and Shelkin (1943) and, since that, this physical mechanism is taken into account by the vast majority of premixed turbulent combustion models. At this level of simplifications, turbulent burning velocity is solely controlled by an increase in the mean area $\overline{A}_f$ of the flame-front surface (wrinkled solid line in Fig. 6.7a) when compared to the area $A_0$ of a mean flame surface (dashed straight line), i.e.,

$$U_t = S_L \frac{\overline{A}_f}{A_0}. \tag{6.57}$$

An increase in $u'$ results in increasing the mean dissipation rate $\overline{\varepsilon} \propto u'^3/L$, decreasing the Kolmogorov length $\eta = (\nu^3/\overline{\varepsilon})^{1/4}$ and time $\tau_\eta = (\nu/\overline{\varepsilon})^{1/2}$ scales, and increasing the magnitude $\tau_\eta^{-1}$ of the highest local stretch rate, which is generated by the Kolmogorov eddies (Pope 2000). Because the local area of the flame-front surface is increased by the local turbulent stretch rates, an increase in $u'$ results in increasing $\overline{A}_f$ and $U_t$. A recent DNS study (Yu et al. 2015) of propagation of an infinitely thin interface in constant-density turbulence characterized by $0.5 \le u'/S_L \le 10$ showed a linear dependence of $U_t$ on $u'$, in line with pioneering predictions by Damköhler (1940) and Shelkin (1943).

At the second, more sophisticated level, the local burning rate is still assumed to be unperturbed[4] and controlled by $S_L$, but finite thickness of flamelets is taken into account, see Fig. 6.7b, thus, introducing several new effects. In particular, the smallest scale wrinkles of an infinitely thin interface are smoothed out in the case of a flamelet of a finite thickness, cf. ellipse A in Fig. 6.7a and its counterpart in Fig. 6.7b. A recent DNS study (Yu and Lipatnikov 2017a) showed that such a smoothing mechanism results in decreasing $U_t$ and bending of the computed $U_t(u')$-curves, with the magnitudes of both effects being increased with decreasing $L/\delta_L$.

Moreover, if heat losses play a role, a flamelet of a finite thickness may be quenched by strong turbulent stretching (Bradley et al. 1992). Such effects are often taken into account by multiplying the RHS of Eq. (6.57) with a stretch factor $G_s = 1 - \mathbb{P}_q$, where $\mathbb{P}_q$ is the probability of local combustion quenching by turbulent stretching. The reader interested in modeling this probability is referred to Bradley et al. (2005).

Furthermore, if the rms turbulent velocity $u'$ is increased, the Kolmogorov length scale $\eta$ is decreased and the Kolmogorov eddies may penetrate into the flamelet

[4] In the case of a single-step chemistry, the local burning rate in an adiabatic laminar premixed flame is not affected by the flame curvature or the local strain rate if (i) the activation temperature of the combustion reaction is asymptotically high, i.e., $\Theta/T_b \gg 1$, and (ii) the mixture is equidiffusive, i.e., $D_F = D_O = \kappa$, e.g., see a review paper by Clavin (1985).

preheat[5] zones and perturb their structure, thus, making the flamelet approximation wrong in such a case. If $u'$ is further increased, the Kolmogorov eddies may become very small and may be able to penetrate even into the reaction zones, thus, intensifying mixing in these zones. By considering the case of $L/\delta_L \ll 1$, Damköhler (1940) assumed that the influence of turbulence on premixed combustion might solely be reduced to an increase in the diffusivity within the flame. Accordingly, turbulent burning velocity may be determined using results of the thermal laminar flame theory (Zel'dovich et al. 1985) and substituting the molecular diffusivity with the turbulent one, i.e.,

$$U_t = S_L \sqrt{\frac{D_t}{\kappa}} \propto S_L \sqrt{\mathrm{Re}_t} \tag{6.58}$$

This scaling is supported by recent DNS data (Yu and Lipatnikov 2017b) obtained from a number of premixed turbulent flames characterized by high Karlovitz and low Damköhler numbers.

On the contrary, if flamelet thickness is sufficiently large, the smallest turbulent eddies may disappear in the flamelet preheat zones due to increased viscous dissipation and dilatation (Poinsot et al. 1991; Roberts et al. 1993). In such a case, the smallest eddies do not affect $U_t$, i.e., the considered dissipation and dilatation effects are somehow similar to the smoothing effect discussed earlier.

Finally, if flamelets of a finite thickness are convected close to one another, they preheated zones may overlap, thus, heating the unburned gas and, subsequently, increasing the local burning rate (Poludnenko and Oran 2011).

Thus, even this brief overview shows that, if a finite thickness of flamelets is taken into account, various physical mechanisms of flame–turbulence interaction may be highlighted. Accordingly, in the literature, a number of different expressions for $U_t$ and the mean rate $\overline{\dot{\omega}_c}$ may be found, as will be illustrated later.

When compared to models that address an infinitely thin flame front, the following feature of models that allow for a finite flamelet thickness appears to be of paramount importance, especially for engine applications. Even if the former models yield different expressions for $U_t$, all these expressions may be subsumed to $U_t = u' f(S_L/u')$ for dimensional reasoning, because these models consider $S_L$ to be a single dimensional combustion characteristic. Here, $f$ is an arbitrary function with its derivative $f' \geq 0$ in order for an increase in $S_L$ to result in increasing or constant $U_t$. Therefore, if the pressure is increased and $u'$ retains the same value, then, these models yield a decreasing or constant $U_t$, because $S_L$ is decreased with increasing $p$ for a typical hydrocarbon–air mixture.

However, as reviewed elsewhere (Lipatnikov 2012; Lipatnikov and Chomiak 2002, 2010), there is a large body of experimental data that cogently show an increase in $U_t$ by $p$. This well-documented effect may play an important role in pis-

[5] Within the framework of the classical thermal theory of laminar premixed combustion (Zel'dovich et al. 1985), a laminar flame consists of a preheat zone, where the reaction rate vanishes, and a significantly thinner reaction zone which heat release is localized to.

ton engines where the pressure strongly varies during the combustion phase, but, as argued above, this effect cannot be predicted by a model that deals with infinitely thin flame fronts.

On the contrary, a model that allows for a finite flamelet thickness and yields an increase in $U_t$ by $L/\delta_L$ may predict the increase in $U_t$ by the pressure. Indeed, $\delta_L \propto \kappa/S_L \propto p^{-1}/p^{-s}$ is decreased with increasing pressure, because the power exponent $s$ in $S_L \propto p^{-s}$ is significantly smaller than unity, e.g. $s \approx 0.5$ or 0.25 for methane or heavier paraffins, respectively. Thus, dependence of turbulent burning rate on flamelet thickness is of substantial importance, especially for CFD research into burning in piston engines.

At the third level of simplification, see Fig. 6.7c, not only a finite flamelet thickness, but also differences in (i) $D_F$ and $D_O$ (the so-called preferential diffusion effects) and (ii) $Le$ and unity (the so-called Lewis number effects) are taken into account. Discussion of such effects is beyond the scope of the present chapter and the interested reader is referred to review paper (Lipatnikov and Chomiak 2005c) and monograph (Lipatnikov 2012). Here, it is worth noting that, if the molecular diffusivity of the deficient reactant, e.g. hydrogen in a lean $H_2$/air mixture, is significantly higher than the diffusivity of another reactant, then, local burning rate in positively curved[6] flamelets may be significantly increased by the preferential diffusion and Lewis number effects, cf. ellipse B and its counterpart in Figs. 6.7b and 6.7c, respectively. The opposite change in the local burning rate is observed (in the considered case of a lean $H_2$/air mixture) in negatively curved flamelets, cf. ellipse C and its counterpart in Figs. 6.7b and 6.7c, respectively.

As reviewed elsewhere (Kuznetsov and Sabelnikov 1990; Lipatnikov 2012; Lipatnikov and Chomiak 2005c), the preferential diffusion and Lewis number effects play a very important role in premixed turbulent combustion even at high $u'/S_L$ and $\mathrm{Re}_t$. In particular, such effects appear to be of great importance when burning renewable fuels such as syngas (Venkateswaran et al. 2011, 2013, 2015).

An important role played by molecular transport even at $D_F/D_t \propto \mathrm{Re}_t^{-1} \ll 1$ might appear to be surprising at first glance. However, it is worth remembering that combustion is localized to thin reaction zones, where a small molecular diffusivity, e.g. $D_F$, is multiplied with a large spatial gradient, e.g., $\nabla Y_F$. Accordingly, in these zones, the molecular transport and reaction terms are of the same order, in line with the thermal theory of laminar premixed combustion (Zel'dovich et al. 1985). Consequently, the preferential diffusion and Lewis number effects may substantially change the local temperature and mixture composition in reaction zones, thus, strongly affecting the local $\dot{\omega}_c$. In the Favre-averaged transport Eq. (6.27), the mean molecular transport term may be significantly smaller than the mean reaction term, because flamelet preheat zones do not contribute to the latter term, but contribute to the former term, with the reaction and preheat zone contributions to the mean molecular transport term counterbalancing one another to the leading order. Nevertheless, the mean reaction rate may straightforwardly depend on $D_F/D_O$ and/or

[6]Curvature is considered to be positive or negative if the curvature center is in burned or unburned gas, respectively.

*Le*, because molecular transport plays an important role in the reaction zones, as noted above.

Finally, it is worth noting that, in the case of single-step chemistry, a single combustion progress variable does not allow us to characterize mixture composition if $D_F \neq D_O$ or $Le \neq 1$. At least two (if $D_F \neq D_O$ and $Le = 1$ or $D_F = D_O$ and $Le \neq 1$) or three (if $D_F \neq D_O$ and $Le \neq 1$) scalar quantities are required to properly characterize the mixture composition in such a case. However, if $\bar{c}$ is considered to be the probability of finding combustion products, a single combustion progress variable and a single transport Eq. (6.27) may be used to simulate premixed turbulent combustion by invoking the two-fluid or BML approximation. In order for such simulations to allow for the preferential diffusion and Lewis number effects, these effects should be properly addressed by the invoked closure relation for $\overline{\dot{\omega}_c}$. An example of such a model will be given in Sect. 6.4.2.

#### 6.3.3.2 Some Approaches to Modeling

The contents of this section are restricted to models developed to obtain a closure relation solely for the source term $\overline{\dot{\omega}_c}$ in Eq. (6.27), whereas a closure relation for the scalar flux $\overline{\rho \mathbf{u}'' c''}$ is assumed to be provided by another model. The most widely used models of the mean rate $\overline{\dot{\omega}_c}$ belong to one of the following three groups; (i) algebraic models, (ii) models that deal with an extra transport equation for the mean Flame Surface Density (FSD) $\overline{|\nabla c|}$, (iii) models that deal with an extra transport equation for the mean Scalar Dissipation Rate (SDR) $\tilde{\chi} = 2\bar{\rho}^{-1}\overline{\rho D \nabla c'' \cdot \nabla c''}$.

Algebraic Models

In the literature, there is a number of different algebraic closure relations for $\overline{\dot{\omega}_c}$, which were obtained invoking different assumptions. All such models may be subsumed to

$$\overline{\dot{\omega}_c} = \frac{\bar{\rho}\Omega}{\tau_f}, \tag{6.59}$$

where a flame time scale $\tau_f$ is introduced for dimensional reasoning and $\Omega = \Omega(\tilde{c}, \bar{\rho}/\rho_u)$ is a function of the normalized density and the mean combustion progress variable $\tilde{c}$ or $\bar{c}$. Since such models usually invoke the BML approach and, in particular, $\bar{\rho}\tilde{c} = \sigma^{-1}\rho_u \bar{c}$, the knowledge of $\bar{\rho}/\rho_u$ and $\tilde{c}$ is equivalent to the knowledge of $\bar{\rho}/\rho_u$ and $\bar{c}$ within the framework of these models.

Examples of expressions for the time scale $\tau_f$ and function $\Omega(\tilde{c}, \bar{\rho}/\rho_u)$, associated with various models, are given in Table 6.1, where $\tau_t = L/u'$ is a turbulence time scale, $Da = \tau_t/\tau_c$ is the Damköhler number, $\tau_c = \delta_L/S_L$ is the laminar flame time scale, $C_1$, $C_2$, and $C_3$ are model constants (values of $C_1$ are different for different models) provided in the cited papers, and the functions $\Gamma(u'/S_L, L/\delta_L)$, $I_0(\mathrm{Re}_t^{1/2}/Da)$, and $\mathscr{F}(\mathrm{Re}_t)$ are also provided in the cited papers, as well as the length scale $\hat{L}_y$.

**Table 6.1** Algebraic models

| $\tau_f^{-1}$ | $\Omega$ | References |
|---|---|---|
| $C_1\Gamma\tau_t^{-1}$ | $\bar{c}(1-\bar{c})$ | Bailly et al. (1997) |
| $C_1\tau_t^{-1}$ | $\bar{\rho}\tilde{c}(1-\tilde{c})/\rho_u$ | Bray (1980) |
| $C_1 l_0 S_L/\hat{L}_y$ | $\bar{c}(1-\bar{c})$ | Bray (1990) |
| $\mathscr{F}\frac{S_L}{u'}\tau_t^{-1}$ | $\bar{c}(1-\bar{c})$ | Lindstedt and Váos (1999) |
| $C_1\left[S_L/u' + \left(1+Da^{-2}\right)^{-1/4}\right]^2\tau_t^{-1}$ | $\bar{\rho}\tilde{c}(1-\tilde{c})/\rho_u$ | Schmidt et al. (1998) |
| $C_1\left(1+C_2 S_L/u'\right)\left(C_3 Da^{-1}+1\right)\tau_t^{-1}$ | $\bar{\rho}\tilde{c}(1-\tilde{c})/\rho_u$ | Swaminathan and Bray (2005) |

Table 6.1 clearly shows that different model expressions are associated with different levels of simplifications. For instance, one of the oldest expressions for $\tau_f$, see the second row in Table 6.1, involves neither laminar flame speed nor the laminar flame thickness. This model is based on an assumption that burning rate is controlled by turbulent mixing rate and, therefore, $\tau_f$ scales as $\tau_t$. However, such a model cannot predict the well-documented and practically important increase in turbulent burning velocity by the pressure (provided that $u'$ and $L$ are not affected by $p$).

Certain models yield an increase in the burning rate by $S_L$, but do not involve the thickness $\delta_L$, e.g., see the fourth row in Table 6.1. Other models involve both $S_L$ and $\delta_L$, but the influence of the thickness of $\overline{\dot{\omega}_c}$ vanishes if $Da \gg 1$, e.g., see the fifth and sixth rows in Table 6.1. Consequently, at high Damköhler numbers, these models yield a decrease in the burning rate with increasing pressure (due to a decrease in $S_L$), contrary to a large amount of experimental data that show an increase in $U_t$ by $p$ (Lipatnikov 2012; Lipatnikov and Chomiak 2002).

As far as capability for predicting the increase in $U_t$ by $p$ is concerned, the expressions listed in the first and third rows in Table 6.1 do yield the correct trend. Therefore, these expressions appear to be most promising. Nevertheless, it is worth stressing that neither of the algebraic models has yet been validated in a solid manner, i.e., by retaining the model constant(s) unchanged, against a wide set of experimental data obtained from substantially different flames under substantially different conditions. While the model addressed in the second row in Table 6.1 was applied to simulating various experiments, significant changes in the model constant $C_1$ were required to reach an agreement with data obtained from different flames.

### Flame Surface Density Models

The most FSD models are based on assumptions that (i) the mass rate $\overline{\dot{\omega}_c}$ of product creation per unit volume is equal to a product of the mean flamelet surface area per this unit volume, i.e., the mean flame surface density $\overline{\Sigma}$, and the mean mass rate $\rho_u \bar{u}_c$ of product creation per the unit area of the flame surface, and (ii) the latter mass rate is approximately equal to $\rho_u S_L$. The former assumption neglects eventual correlations between $\Sigma$ and $\rho_u u_c$. The latter assumption neglects perturbations of the local flamelet structure and the local burning rate by turbulent eddies and, therefore, may be valid in sufficiently weak turbulence only.

The foundations of the FSD approach can be illustrated by rewriting Eq. (6.23) as follows:

$$\frac{\partial}{\partial t}(\rho c) + \nabla \cdot (\rho \mathbf{u} c) = \rho S_d |\nabla c| \tag{6.60}$$

where $S_d$ defined as follows:

$$S_d \equiv \frac{\nabla \cdot (\rho D \nabla c) + \dot{\omega}_c}{\rho |\nabla c|} \tag{6.61}$$

is the so-called displacement speed in the case of a finite flamelet thickness.[7] The displacement speed is the speed of motion of an iso-scalar surface with respect to the local flow. Indeed, using Eq. (6.2), Eq. (6.60) reads

$$\frac{\partial c}{\partial t} = \left(S_d + \mathbf{n} \cdot \mathbf{u}\right) |\nabla c| \tag{6.62}$$

in the case of a finite flamelet thickness.

The Favre-averaged Eq. (6.60) reads

$$\frac{\partial}{\partial t}(\bar{\rho}\tilde{c}) + \nabla \cdot (\bar{\rho}\tilde{\mathbf{u}}\tilde{c}) = -\nabla \cdot \overline{\rho \mathbf{u}'' c''} + \overline{\rho S_d |\nabla c|}. \tag{6.63}$$

Subsequently, if we assume that equality of $\rho S_d = \rho_u S_L$ holds not only in the unperturbed laminar flame, but also in turbulent flames, then, we arrive at

$$\frac{\partial}{\partial t}(\bar{\rho}\tilde{c}) + \nabla \cdot (\bar{\rho}\tilde{\mathbf{u}}\tilde{c}) = -\nabla \cdot \overline{\rho \mathbf{u}'' c''} + \rho_u S_L \overline{|\nabla c|}. \tag{6.64}$$

Comparison of Eqs. (6.27) and (6.64) shows

$$\overline{\nabla \cdot (\rho D \nabla c) + \dot{\omega}_c} = \rho_u S_L \overline{|\nabla c|} \tag{6.65}$$

or

$$\overline{\dot{\omega}_c} \approx \rho_u S_L \overline{|\nabla c|} \tag{6.66}$$

if the molecular transport term is neglected at high Reynolds numbers. Equation (6.66) is the cornerstone of the FSD approach, as the straightforward relation between FSD $\Sigma$ and $|\nabla c|$ is well established, as reviewed elsewhere (Poinsot and Veynante 2005; Veynante and Vervisch 2002).

Transport equations for $\Sigma$ were derived using different methods (Candel and Poinsot 1990; Pope 1988; Trouvé and Poinsot 1994; Vervisch et al. 1995; Zimont 2015). After averaging such equations involve a set of unclosed terms that should be modeled. There are different models of that kind, but all of them may be subsumed

[7] A product of $\rho|\nabla c|$ is mathematically meaningless in the case of an infinitely thin flame front, because both $\rho$ and $|\nabla c|$ are discontinuous at the front.

**Table 6.2** Flame surface density models

| Source term $\mathscr{P}$ | Sink term $\mathscr{D}$ | Model |
|---|---|---|
| $C_1 \left(\frac{\tilde{\varepsilon}}{\nu}\right)^{1/2} \overline{\Sigma}$ | $C_2 S_L \frac{2+e^{-C_3 R}}{3(1-\bar{c})} \overline{\Sigma}^2$, where $R = \frac{(1-\bar{c})\tilde{\varepsilon}}{S_L \overline{\Sigma}\tilde{k}}$ | Cant et al. (1990) |
| $C_1 \frac{\tilde{\varepsilon}}{\tilde{k}} \overline{\Sigma}$ | $C_2 \frac{S_L}{1-\bar{c}} \overline{\Sigma}^2$ | CFM (Candel et al. 1990; Fichot et al. 1993) |
| $C_1 \frac{\tilde{\varepsilon}}{\tilde{k}} \overline{\Sigma}$ | $C_2 \frac{S_L + C_3 u'}{1-\bar{c}} \overline{\Sigma}^2$ | CFM1 (Candel et al. 1990; Duclos et al. 1993) |
| $C_1 \Gamma \frac{\tilde{\varepsilon}}{\tilde{k}} \overline{\Sigma}$ | $C_2 \frac{S_L + C_3 u'}{1-\bar{c}} \overline{\Sigma}^2$ | CFM2a (Boudier et al. 1992) |
| $C_1 \Gamma \frac{\tilde{\varepsilon}}{\tilde{k}} \overline{\Sigma}$ | $C_2 \frac{S_L + C_3 u'}{\bar{c}(1-\bar{c})} \overline{\Sigma}^2$ | CFM2b (Duclos et al. 1993) |
| $C_1 \frac{\tilde{\varepsilon}}{\tilde{k}} \overline{\Sigma}$ if $Da \geq C_2$ | $C_3 \frac{S_L}{1-\bar{c}} \overline{\Sigma}^2$ | Cheng and Diringer (1991) |
| $C_1 \left(\frac{\tilde{\varepsilon}}{\nu}\right)^{1/2} \overline{\Sigma}$ | $C_2 \frac{\rho_u S_L}{\bar{\rho}\bar{c}(1-\bar{c})} \overline{\Sigma}^2$ | Choi and Huh (1998) |
| $C_1 \frac{u'}{l_r} \overline{\Sigma}$ | $C_2 \frac{\rho_u S_L}{\bar{\rho}\bar{c}(1-\bar{c})} \overline{\Sigma}^2$ | Lee et al. (1998) |

to

$$\frac{\partial \overline{\Sigma}}{\partial t} + \nabla \cdot \left(\tilde{\mathbf{u}} \overline{\Sigma}\right) = \nabla \cdot \left(\frac{\nu_t}{Sc_t} \nabla \overline{\Sigma}\right) + \mathscr{P} - \mathscr{D}, \tag{6.67}$$

with the source $\mathscr{P}$ and consumption $\mathscr{D}$ terms being specified in Table 6.2. Here, $Sc_t$ and $C_j$ are constants, which may be different for different models, $\tilde{k}$ and $\tilde{\varepsilon}$ are the Favre-averaged turbulent kinetic energy and its dissipation rate, respectively, $\nu_t$ is the turbulent viscosity given by a turbulence model, $\Gamma = \Gamma(u'/S_L, L/\Delta_L)$ is the so-called efficiency function[8] introduced by Meneveau and Poinsot (1991), and $l_r$ is a dimensional constant (a length scale).

While the FSD models are widely used in applied CFD research into premixed turbulent combustion in engines, there is a need for thoroughly validating such models against a wide set or representative experimental data obtained from various well-defined simple flames under substantially different conditions.

Moreover, the FSD models suffer from fundamental limitations. In particular, first, the validity of the cornerstone Eq. (6.65) and its simplified version given by Eq. (6.66) may be put into question even in weakly turbulent flames commonly associated with the flamelet combustion regime and minor perturbations of local flamelet structure and burning rate $\rho u_c$ by turbulent eddies. For instance, dashed line in Fig. 6.8 shows that a ratio of $\overline{\dot{\omega}_c}/(\rho_u S_L |\overline{\nabla c}|)$ is significantly increased by $\bar{c}$ at $\bar{c} < 0.2$ and $0.8 < \bar{c}$. At low $\bar{c}$, variations in a ratio of $\overline{(\nabla \cdot (\rho D \nabla c) + \dot{\omega}_c)}/(\rho_u S_L |\overline{\nabla c}|)$, see solid line, are less pronounced, but they are still substantial at $0.8 < \bar{c}$. Therefore, neither Eq. (6.65) nor Eq. (6.66) holds under conditions of this DNS study (Lipat-

[8] There is the same function in Table 6.1 also.

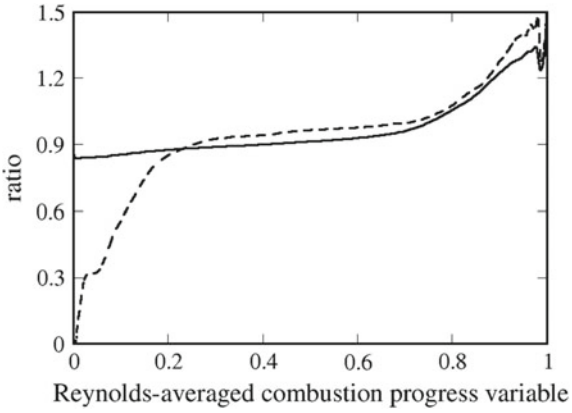


**Fig. 6.8** Ratios of $\overline{\dot{\omega}_c}/(\rho_u S_L|\overline{\nabla c}|)$ (dashed line) and $\overline{(\nabla\cdot(\rho D\nabla c)+\dot{\omega}_c)}/(\rho_u S_L|\overline{\nabla c}|)$ (solid line) obtained in a DNS study (Lipatnikov et al. 2017) of weakly turbulent premixed burning associated with the flamelet combustion regime (Peters 2000)

nikov et al. 2017) in spite of the facts that (i) these conditions are well associated with the flamelet regime of premixed turbulent combustion and (ii) at least one of the two aforementioned equations is commonly assumed to be valid in the flamelet combustion regime.

Second, closure relations summarized in Table 6.2 involves the unperturbed laminar flame speed $S_L$, but do not allow for the influence of local flamelet perturbations on the balance of the mean FSD within a premixed turbulent flame brush. However, the already cited DNS study (Lipatnikov et al. 2017) shows that such an influence is of substantial importance and should be addressed properly.

Scalar Dissipation Rate Models

The SDR models are based on the following linear relation:

$$\overline{\dot{\omega}_c} = \frac{\bar{\rho}\tilde{\chi}}{2c_m - 1}, \tag{6.68}$$

where

$$c_m = \frac{\overline{c\dot{\omega}_c}}{\overline{\dot{\omega}_c}} \tag{6.69}$$

is commonly assumed to be a constant larger than 0.5.

Within the framework of the BML approach, Eqs. (6.68) and (6.69) can be derived straightforwardly (Bray 1979). First, multiplication of Eq. (6.23) with $c$ yields

$$\frac{\partial}{\partial t}\left(\rho c^2\right) + \nabla\cdot\left(\rho\mathbf{u}c^2\right) = 2c\nabla\cdot(\rho D\nabla c) + 2c\dot{\omega}_c \tag{6.70}$$

using Eq. (6.2). Second, the Favre-averaged Eq. (6.70) reads

$$\frac{\partial}{\partial t}\left(\bar{\rho}\tilde{c}^2\right)+\frac{\partial}{\partial t}\left(\overline{\rho c''^2}\right)+\nabla\cdot\left(\bar{\rho}\tilde{\mathbf{u}}\tilde{c}^2\right)+\nabla\cdot\left(\tilde{\mathbf{u}}\overline{\rho c''^2}\right)+2\nabla\cdot\left(\tilde{c}\overline{\rho\mathbf{u}''c''}\right)$$
$$+\nabla\cdot\overline{\rho\mathbf{u}''c''^2}=2\tilde{c}\nabla\cdot\overline{(\rho D\nabla c)}+2\overline{c''\nabla\cdot(\rho D\nabla c)}+2\tilde{c}\overline{\dot{\omega}_c}+2\overline{c''\dot{\omega}_c}. \quad (6.71)$$

Third, multiplication of Eq. (6.27) with $\tilde{c}$ yields

$$\frac{\partial}{\partial t}\left(\bar{\rho}\tilde{c}^2\right)+\nabla\cdot\left(\bar{\rho}\tilde{\mathbf{u}}\tilde{c}^2\right)+2\tilde{c}\nabla\cdot\overline{\rho\mathbf{u}''c''}=2\tilde{c}\nabla\cdot\overline{(\rho D\nabla c)}+2\tilde{c}\overline{\dot{\omega}_c}. \quad (6.72)$$

Fourth, subtraction of Eq. (6.72) from Eq. (6.71) results in

$$\frac{\partial}{\partial t}\left(\overline{\rho c''^2}\right)+\nabla\cdot\left(\tilde{\mathbf{u}}\overline{\rho c''^2}\right)$$
$$=-2\overline{\rho\mathbf{u}''c''}\cdot\nabla\tilde{c}-\nabla\cdot\overline{\rho\mathbf{u}''c''^2}+2\overline{c''\nabla\cdot(\rho D\nabla c)}+2\overline{c''\dot{\omega}_c}. \quad (6.73)$$

Fifth, within the framework of the BML approach, we have

$$\begin{aligned}\overline{\rho\mathbf{u}''c''^2}&=\rho_u(1-\tilde{c})\left(\tilde{\mathbf{u}}_u-\tilde{\mathbf{u}}\right)\tilde{c}^2+\rho_b\tilde{c}\left(\tilde{\mathbf{u}}_b-\tilde{\mathbf{u}}\right)(1-\tilde{c})^2\\&=\bar{\rho}\tilde{c}(1-\tilde{c})\left[\tilde{c}\left(\tilde{\mathbf{u}}_u-\tilde{\mathbf{u}}\right)+(1-\tilde{c})\left(\tilde{\mathbf{u}}_b-\tilde{\mathbf{u}}\right)\right]\\&=\bar{\rho}\tilde{c}(1-\tilde{c})\left[\tilde{c}\tilde{\mathbf{u}}_u+(1-\tilde{c})\tilde{\mathbf{u}}_b-\tilde{\mathbf{u}}\right]\\&=\bar{\rho}\tilde{c}(1-\tilde{c})\left[\tilde{c}\tilde{\mathbf{u}}_u+(1-\tilde{c})\tilde{\mathbf{u}}_b-(1-\tilde{c})\tilde{\mathbf{u}}_u-\tilde{c}\tilde{\mathbf{u}}_b\right]\\&=\bar{\rho}\tilde{c}(1-\tilde{c})\left(\tilde{\mathbf{u}}_b-\tilde{\mathbf{u}}_u\right)(1-2\tilde{c})=\overline{\rho\mathbf{u}''c''}(1-2\tilde{c}).\end{aligned} \quad (6.74)$$

Sixth, substitution of Eqs. (6.37), (6.41), (6.69) and (6.74) into Eq. (6.73) yields

$$(1-2\tilde{c})\frac{\partial}{\partial t}(\bar{\rho}\tilde{c})+(1-2\tilde{c})\nabla\cdot(\bar{\rho}\tilde{\mathbf{u}}\tilde{c})$$
$$=-(1-2\tilde{c})\nabla\cdot\overline{\rho\mathbf{u}''c''}+2\overline{c''\nabla\cdot(\rho D\nabla c)}+2(c_m-\tilde{c})\overline{\dot{\omega}_c} \quad (6.75)$$

using Eq. (6.15). Seventh, subtraction of Eq. (6.27) multiplied with $(1-2\tilde{c})$ from Eq. (6.75) results in

$$\begin{aligned}\left(2c_m-1\right)\overline{\dot{\omega}_c}&=-2\overline{c''\nabla\cdot(\rho D\nabla c)}+(1-2\tilde{c})\nabla\cdot\overline{(\rho D\nabla c)}\\&=2\overline{\rho D\nabla c\cdot\nabla c''}-2\nabla\cdot\overline{(\rho c''D\nabla c)}+(1-2\tilde{c})\nabla\cdot\overline{(\rho D\nabla c)}\\&=\bar{\rho}\tilde{\chi}+2\overline{\rho D\nabla c''}\cdot\nabla\tilde{c}-2\nabla\cdot\overline{(\rho c''D\nabla c)}+(1-2\tilde{c})\nabla\cdot\overline{(\rho D\nabla c)}.\end{aligned} \quad (6.76)$$

At $\mathrm{Re}_t\gg 1$ and $Da\gg 1$, instantaneous variations in $c$ are localized to thin flamelets characterized by large (when compared to $|\nabla\tilde{c}|$) spatial gradients $|\nabla c|$. Consequently, the first term on the RHS of Eq. (6.76) scales as $\delta_L^{-2}$ and dominates, whereas other terms scale as $\delta_t^{-1}\delta_L^{-1}$. Therefore, by neglecting $O(\delta_t^{-1}\delta_L^{-1})$-order terms, we arrive at Eq. (6.68).

Equations (6.68) and (6.69) offer an opportunity to evaluate the mean rate $\overline{\dot{\omega}_c}$ by studying a transport equation for the Favre-averaged scalar dissipation rate $\tilde{\chi}$. Such an approach was pioneered by Borghi (1990) who derived a transport equation for $\bar{\chi}$ in the case of a constant density. Subsequently, Swaminathan and Bray (2005) derived a transport equation for $\tilde{\chi}$ in the case of variable density. In both cases, the transport equations involve a number of terms that require closure relations.

Models of these terms were developed by a few research groups, as reviewed elsewhere (Chakraborty et al. 2011). In all applications of these models, $c_m$ was assumed to retain the same value in the entire flame brush and this assumption was supported in a recent DNS study (Lipatnikov et al. 2015a). However, $c_m$ is not a constant and may depend e.g. on the choice of a combustion progress variable (Lipatnikov et al. 2015a).

The discussed SDR approach definitely requires more validation studies. In particular, capabilities of the SDR models for predicting an increase in $U_t$ by the pressure should be tested. The point is that equations written in the bottom row in Table 6.1 were obtained using a SDR model (Swaminathan and Bray 2005), but these equations appear to yield a wrong trend, i.e., a decrease in $U_t$ with increasing $p$, if $Da \gg 1$.

Moreover, since Eq. (6.68) was derived within the framework of the BML paradigm, the SDR approach seems to be best justified in the flamelet combustion regime. However, DNS data obtained from weakly turbulent flames associated with the flamelet combustion regime (Lipatnikov et al. 2015a) and plotted in Fig. 6.9a show that a ratio of $\overline{\dot{\omega}_c}/(\bar{\rho}\tilde{\chi})$ is increased by $\bar{c}$, whereas $c_m$ evaluated using Eq. (6.69) is close to 0.9 in the largest parts of all three flame brushes, see Fig. 6.9b. Therefore, Fig. 6.9 does not support Eq. (6.68), with the differences between the model and DNS results being most pronounced at the trailing and, especially, leading edge of the mean flame brush. Inability of Eq. (6.68) to yield the correct value of the mean rate $\overline{\dot{\omega}_c}$ at $\bar{c} \ll 1$ is a serious limitation, because the leading edge of a premixed turbulent flame brush may play a crucial role in the flame propagation, as discussed in detail elsewhere (Kuznetsov and Sabelnikov 1990; Lipatnikov 2012; Lipatnikov and Chomiak 2005c; Sabelnikov and Lipatnikov 2013, 2015; Zel'dovich et al. 1985).

Thus, as far as models that invoke an extra transport equation for $\overline{\Sigma}$ or $\tilde{\chi}$ are concerned, a basic weak point of such models consists of the fact that neither the linear Eq. (6.66) nor the linear Eq. (6.68) is a sufficiently precise closure relation even under conditions that are well associated with its derivation.

Alternatively, transport equations for $\dot{\omega}_c$ and $\overline{\dot{\omega}_c}$ can be derived straightforwardly. Such an approach was recently put forward and already yielded encouraging results (Sabelnikov et al. 2016, 2017). Nevertheless, discussion of this new approach is beyond the scope of the present chapter, because a completely closed transport equation for $\overline{\dot{\omega}_c}$ has not yet been elaborated.

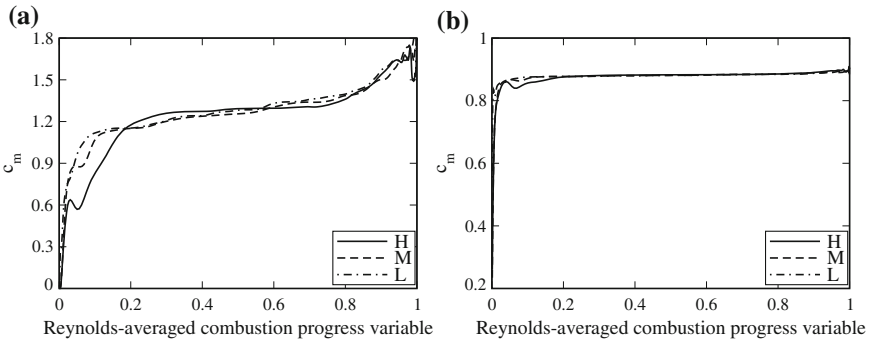


**Fig. 6.9** **a** Ratios of $\overline{\dot{\omega}_c}/(\bar{\rho}\tilde{\chi})$ and **b** $c_m$ obtained from three statistically planar 1D flames in a DNS study (Lipatnikov et al. 2015a) of weakly turbulent premixed burning associated with the flamelet combustion regime (Peters 2000). Flames H, M, and L are characterized by the density ratio $\sigma = 7.53$, 5.0, and 2.5, respectively

## 6.4 Turbulent Flame Closure and Flame Speed Closure Models

The goal of the present section is to discuss (i) the so-called Turbulent Flame Closure (TFC) model of the influence of turbulence on premixed burning and (ii) its extension known as Flame Speed Closure (FSC) model. These models are selected for a more detailed discussion, because they have yet been validated using a significantly wider set of experimental data obtained from well-defined simple cases when compared to any competing model developed for RANS simulations of premixed turbulent combustion.

### *6.4.1 Equations*

TFC Model

The foundations of the TFC model were laid in the pioneering work by Prudnikov (1960, 1964). Subsequently, the model was developed by Zimont (1979). The final version of the TFC model, which is implemented in various commercial CFD codes, was presented by Karpov et al. (1996) and Zimont and Lipatnikov (1995).

The TFC model deals with the following closed transport equation

$$\frac{\partial}{\partial t}\left(\bar{\rho}\tilde{c}\right) + \nabla \cdot \left(\bar{\rho}\tilde{\mathbf{u}}\tilde{c}\right) = \nabla \cdot \left[\bar{\rho}(\kappa + D_t)\nabla\tilde{c}\right] + \rho_u U_t \left|\nabla\tilde{c}\right|, \tag{6.77}$$

i.e., the model provides the following joint closure relation

$$-\nabla\cdot\overline{\rho\mathbf{u}''c''}+\overline{\dot{\omega}_c}=\nabla\cdot[\bar{\rho}(\kappa+D_t)\nabla\tilde{c}]+\rho_u U_t\,|\nabla\tilde{c}| \tag{6.78}$$

for the two terms on the RHS of Eq. (6.27). The molecular heat diffusivity $\kappa$ of the mixture is commonly neglected when compared to the turbulent diffusivity $D_t$ when using the TFC model.

Equation (6.77) was in fact introduced into the combustion literature by Prudnikov (1960, 1964), but he wrote it in another form and applied it solely to statistically planar 1D flame that propagated in frozen turbulence. In the same 1D case, Eq. (6.77) was derived by Lipatnikov and Chomiak (2005a, b) by assuming that the mean structure of a developing premixed turbulent flame was self-similar,[9] in line with various experimental data analyzed elsewhere (Lipatnikov 2012; Lipatnikov and Chomiak 2000b, 2001, 2002, 2004; Prudnikov 1964).

Equation (6.77) yields permanent growth of the mean thickness $\delta_t$ of the statistically planar 1D flame, whereas turbulent burning velocity does not depend on time to the leading order (Prudnikov 1964). Such an intermediately asymptotic regime of premixed turbulent combustion pointed out by Prudnikov (1964), Kuznetsov (1975), Clavin and Williams (1979), and Zimont (1979) was later called "intermediate steady propagation (ISP) flames" (Zimont 2000).

In order to be consistent with this basic peculiarity of Eq. (6.77), a model for the turbulent burning velocity $U_t$, required to close the approach, should also address the ISP flames. To the best of the present author's knowledge, the sole model that satisfies this basic requirement has yet been developed by Zimont (1979), who has theoretically obtained the following expression:

$$U_{t,ISP}=Au'Da^{1/4}=Au'\left(\frac{\tau_t}{\tau_c}\right)^{1/4}=Au'^{3/4}S_L^{1/2}L^{1/4}\kappa_u^{-1/4}, \tag{6.79}$$

with $U_t=U_{t,ISP}$ being substituted into the second term on the RHS of Eq. (6.77) within the framework of the TFC model. Here, $A$ is a single model constant. Equation (6.79) was derived under the following constraints (Zimont 1979, 2000); (i) the turbulent Reynolds number $\mathrm{Re}_t=u'L/\nu_u\gg 1$, (ii) the Damköhler number $Da\gg 1$, (iii) the Karlovitz number $Ka\propto(u'/S_L)^2\mathrm{Re}_t^{-1/2}>1$, and (iv) the flame-development time $\tau_t<t_{fd}\ll\tau_t Da^{3/2}$. Subsequent tests of the TFC model have shown that it works well in a wider range of conditions, e.g., (ii′) $Da>1$ and (iii′) $u'>S_L$.

The reader interested in further discussion of the foundations of the TFC model is referred to Lipatnikov (2012), Lipatnikov and Chomiak (2002) and Zimont (2000).

To the best of the present author's knowledge, in all RANS applications of the TFC model, (i) the turbulent diffusivity $D_t$ in the first term on the RHS of Eq. (6.77) was associated with the fully developed turbulent diffusivity $D_{t,\infty}$ yielded by a turbulence model, e.g.

$$D_{t,\infty}=\frac{C_\mu}{Sc_t}\frac{\tilde{k}^2}{\tilde{\varepsilon}} \tag{6.80}$$

[9] This feature of premixed turbulent burning will be discussed in Sect. 6.4.4.

if the $k$-$\varepsilon$ model (Launder and Spalding 1972) is invoked, and (ii) the mean density was evaluated using Eq. (6.35). Here, $C_\mu = 0.09$ is a constant of the $k$-$\varepsilon$ model (Launder and Spalding 1972) and $Sc_t$ is a turbulent Schmidt number. Note that Eq. (6.35) is valid not only within the framework of the BML paradigm, but also in a general case provided that $c = (T - T_u)/(T_b - T_u)$, $\rho T = \rho_u T_u$, and, therefore, $1 + (\sigma - 1)c = \rho_u/\rho$. Indeed, Favre averaging of the latter equality results in Eq. (6.35).

FSC Model

The FSC model is strongly based on the TFC model and involves Eqs. (6.77)–(6.79). In addition, the FSC model extends the TFC model in order to simulate an early stage of premixed turbulent flame development and weakly turbulent flames, as discussed in the rest of the present section.

Within the framework of the FSC model, growth of turbulent diffusivity and burning velocity during an early stage of premixed flame development is addressed following the classical theory of turbulent mixing by Taylor (1935), which yields the following well-known expression (Brodkey 1967; Hinze 1975)

$$D_t = D_{t,\infty}\left[1 - \exp\left(-\theta_{fd}\right)\right] \equiv D_{t,\infty} f_1(\theta_{fd}) \tag{6.81}$$

for developing turbulent diffusivity in the simple case of a single point source of admixture. Subsequently, the following expression

$$U_t = U_{t,ISF}\left\{1 + \theta_{fd}^{-1}\left[\exp\left(-\theta_{fd}\right) - 1\right]\right\}^{1/2} \equiv U_{t,ISF} f_2(\theta_{fd}) \tag{6.82}$$

for developing turbulent burning velocity was derived (Lipatnikov and Chomiak 1997) by combining the Taylor theory and the aforementioned model of $U_{t,ISF}$ by Zimont (1979). Here, $\theta_{fd} = t_{fd} u'^2/D_{t,\infty} = t_{fd}/\tau_L$ is the normalized flame-development time $t_{fd}$, $\tau_L$ is the Lagrangian time scale of the turbulence, while $U_{t,ISF}$ and $D_{t,\infty}$ are modeled using Eqs. (6.79) and (6.80), respectively.

The two extra terms $f_1(\theta_{fd})$ and $f_2(\theta_{fd})$, which pertain to the FSC model and describe the development of turbulent diffusivity and burning velocity, respectively, do not involve an empirical or tuning parameter. Both time-dependent terms tend to unity as $\theta_{fd} \to \infty$, i.e., the FSC Eqs. (6.81) and (6.82) reduce to the TFC Eqs. (6.80) and (6.79), respectively, in this limiting case.

The flame-development time can easily be determined in the case of unsteady combustion initiated by a single spark. In such a case, $t_{fd}$ is simply counted from the ignition instant. When modeling a statistically stationary premixed turbulent flame, $t_{fd}$ is still a meaningful quantity. Indeed, a statistically stationary flow can be a developing process, with the development occurring as a fluid particle is convected by the mean flow. Statistically stationary turbulence behind a grid develops, i.e., decays in the direction of the mean flow. A statistically stationary mixing layer develops, i.e., grows in the direction of the mean flow. Similarly, a statistically stationary premixed turbulent flame develops, i.e., both flame speed and mean flame brush thick-

ness grow in the direction of the mean flow. In these cases, the turbulence (layer, or flame, respectively) development time is a meaningful quantity, which is equal to the time required in order for a fluid particle to be convected from the grid (cross section associated with start of the mixing, or cross section where the flame is stabilized, respectively) to the considered point.

It is worth noting that development of turbulent burning velocity can also be of importance for thermoacoustic applications, e.g., (Lipatnikov and Sathiah 2005).

In the simplest case of a statistically planar, 1D flow with frozen turbulence characteristics, the burning velocity $U_t$ yielded by the TFC model scales as $u'Da^{1/4}$ and vanishes as $u' \to 0$. Accordingly, the source term on the RHS of Eq. (6.77) also vanishes in this limiting case, i.e., the TFC model cannot be applied to such a weakly turbulent flame. To resolve the problem, the following laminar-like source term

$$Q_L = \frac{\bar{\rho}(1-\tilde{c})}{t_{ch}(1+D_t/\kappa_b)} \exp\left(-\frac{\Theta}{\tilde{T}}\right) \tag{6.83}$$

was incorporated (Lipatnikov and Chomiak 1997, 2000a, 2002) into the RHS of Eq. (6.77), which reads

$$\frac{\partial}{\partial t}(\bar{\rho}\tilde{c}) + \nabla \cdot (\bar{\rho}\tilde{\mathbf{u}}\tilde{c}) = \nabla \cdot [\bar{\rho}(\kappa + D_t)\nabla \tilde{c}] + \rho_u U_t |\nabla \tilde{c}| + Q_L \tag{6.84}$$

within the framework of the FSC model. Here, $t_{ch}$ and $\Theta$ are the time scale and activation temperature, respectively, of a single reaction that combustion chemistry is reduced to, and the Favre-averaged temperature can easily be evaluated using the ideal gas state equation, e.g., $\bar{\rho}\tilde{T} = \rho_u T_u$. In intense turbulence associated with $\mathrm{Re}_t \to \infty$, a ratio of $D_t/\kappa_b \to \infty$ and, therefore, $Q_L$ vanishes. In this limiting case, the sole difference between the FSC and TFC models is associated with the two time-dependent terms on the RHSs of Eqs. (6.81) and (6.82).

If the laminar flame speed is known, then, the extra source term $Q_L$ given by Eq. (6.83) does not involve a tuning parameter, because the time scale $t_{ch}$ can easily be determined within the framework of the FSC model before running simulations of turbulent combustion. Indeed, if a value of $\Theta$ is set, then, $t_{ch}$ can be evaluated by (i) applying the FSC model to a planar 1D flame in the case of $u' = 0$ and (ii) finding $t_{ch}$ such that the computed flame speed is equal to $S_L$, which is the key input parameter of both the TFC and FSC models. Because the computed flame speed scales as $(\kappa_u/t_{ch})^{1/2}$ (Zel'dovich et al. 1985) if $u' = 0$, the pre-calculation of $t_{ch}$ based on a known $S_L$ requires only two iterations.

If (i) the simplest case of a statistically planar, 1D flame that propagates in frozen turbulence is addressed, (ii) the problem is considered in a coordinate framework that moves at a speed equal to $U_t$ in the direction from the burned to the unburned gas, and (iii) $\kappa + D_t$ and $t_{ch}(1 + D_t/\kappa_b)$ are substituted with $\kappa'$ and $t'_{ch}$, respectively, then, Eqs. (6.83) and (6.84) reduce to the basic equation of the thermal laminar flame theory (Zel'dovich et al. 1985). Consequently, the flame speed is equal to $S_L$ in that coordinate framework (Lipatnikov and Chomiak 1997, 2002). Coming back to the

coordinate framework attached to the mean flow of the unburned gas, we see that the flame speed is equal to $U_t + S_L$ and tends to $S_L$ as $u' \to 0$. Moreover, when $u' \to 0$, the turbulent diffusivity $D_t \to 0$ and the FSC Eq. (6.84) reduces to a well-known simple balance equation that models a laminar premixed flame in the case of a single-step chemistry (Zel'dovich et al. 1985). Thus, the extra source term $Q_L$ results solely from the linear interpolation between the latter balance equation valid at $u' = 0$ and the TFC balance equation valid at $Ka > 1$ or at least $u' > S_L$.

It is worth noting that the use of the extra source term $Q_L$ allows us not only apply the FSC model to weakly turbulent combustion, but also resolves the following problem, which may be of substantial importance in applications. The point is that Eq. (6.77) admits a trivial solution of $\tilde{c}(\mathbf{x}, t)$ =const if boundary conditions are set using $\nabla\tilde{c}$. Accordingly, in order for simulations to yield $\tilde{c} = 1$ somewhere at each instant, at least one boundary condition should be $\tilde{c} = 1$. On the contrary, due to the extra source $Q_L$, Eq. (6.84) is compatible with both types of boundary conditions.

Side by side with the advantages discussed above, the use of $Q_L > 0$ has disadvantages. First, the RHS of Eq. (6.83) is a highly nonlinear function of the mean temperature $\tilde{T}$. Accordingly, if the term $Q_L$ plays a substantial role, it should be resolved using a significantly finer mesh when compared to a mesh required to numerically solve Eq. (6.77).

Second, as discussed in Sect. 6.4.3, the TFC Eq. (6.77) admits an exact analytical solution in a statistically planar 1D case if $D_t$ and $U_t$ are assumed to be constant. This exact solution allows us to easily reveal certain basic features of the TFC model. Such a method of a qualitative analysis cannot be applied straightforwardly to Eq. (6.84) with $Q_L > 0$. Nevertheless, because numerical simulations indicate that the basic features of the TFC and FSC models are similar (with a single exception discussed later), investigation of the basic features of the TFC model sheds some light on the basic features of the FSC model also.

Finally, it is worth noting that the influence of the extra source term $Q_L$ on the computed heat-release rate and mean flame brush thickness is reduced with increasing $u'$. Accordingly, this term may be skipped in simulations of sufficiently intense turbulence provided that the boundary conditions involve $\tilde{c} = 1$ somewhere.

### 6.4.2 Extensions

When performing the first tests of the TFC model (Karpov et al. 1996; Zimont and Lipatnikov 1993, 1995), it was extended by invoking submodels of two well-documented effects that are not addressed by the TFC model. Such a method allowed those researchers to extend the domain of applicability of the TFC model and to test it against a significantly wider set of experimental data. The same two submodels may also be incorporated into the FSC model. It is worth stressing, however, that the two submodels invoked to extend the TFC or FSC model are totally independent and may be either switched on or switched off when necessary.

Local Flame Quenching

In order to address local combustion quenching by intense turbulent stretching, which is discussed in detail elsewhere (Abdel-Gayed et al. 1984; Bradley 1992, 2002; Bradley et al. 1992; Bray 1987; Bray and Cant 1991; Lipatnikov 2012; Lipatnikov and Chomiak 2005c), a stretch factor $G_s = (1 - \mathbb{P}_q)$ may be incorporated into Eq. (6.79), which reads

$$U_{t,ISP} = Au'^{3/4} S_L^{1/2} L^{1/4} \kappa_u^{-1/4} (1 - \mathbb{P}_q), \tag{6.85}$$

where

$$\mathbb{P}_q = 1 - \frac{1}{2} \mathrm{erfc} \left\{ -\frac{1}{\sqrt{2}\sigma_\varepsilon} \left[ \ln \frac{\varepsilon_q}{\tilde{\varepsilon}} + \frac{\sigma_\varepsilon^2}{2} \right] \right\} \tag{6.86}$$

is the probability of local combustion quenching by turbulent strains, erfc is the complementary error function, $\sigma_\varepsilon^2 = 0.26 \ln(L/\eta)$, $\eta = (\nu_u^3/\varepsilon)^{1/4}$ is the Kolmogorov length scale, $\varepsilon_q = 15 \nu_u \dot{s}_q^2$, and $\dot{s}_q$ is a critical stretch rate associated with the local combustion quenching. Equation (6.86) was invented by Bray (1987).

Due to strong sensitivity of a stretched laminar premixed flame to the flame topology and transient effects (Lipatnikov and Chomiak 2005c), a model capable for predicting $\dot{s}_q$ in turbulent flows has not yet been developed. Accordingly, the critical stretch rate is in fact an unknown input parameter of the quenching submodel given by Eq. (6.86). Therefore, the use of that submodel makes simulation results dependent on a tuned value of $\dot{s}_q$, whereas the original TFC model involves a single unknown input parameter, i.e., the constant $A$ in Eq. (6.79), which may be set equal to the same value $A = 0.5$ for various significantly different flames. In all simulations discussed in the following, $\mathbb{P}_q = 0$ unless the opposite is stated.

Preferential Diffusion and Lewis Number Effects

Discussion of effects that stem from differences in molecular transport coefficients of fuel, oxygen, and heat is beyond the scope of the present chapter and the interested reader is referred to books (Kuznetsov and Sabelnikov 1990; Lipatnikov 2012), a review article (Lipatnikov and Chomiak 2005c), and recent papers (Goulier et al. 2017; Venkateswaran et al. 2011, 2013, 2015). Here, it is worth only noting that such effects could be addressed by the TFC or FSC model by substituting the standard chemical time scale $\tau_c$ in Eq. (6.79) with a time scale that characterizes local burning rate in critically perturbed laminar flames. Following Kuznetsov and Sabelnikov (1990), Zimont and Lipatnikov (1993, 1995) used a time scale that characterized burning rate in critically strained planar laminar flames. Subsequently, Karpov and Lipatnikov (1995, 1997) suggested to use another time scale that characterized burning rate in critically curved spherical laminar flames. In particular, that time scale was invoked in a validation study by Karpov et al. (1996), which will be discussed later.

### 6.4.3 Features

Let us consider a statistically planar 1D flame that propagates in homogeneous turbulence from left to right and does not affect the turbulence, i.e., $u'$, $L$, and $D_t$ are assumed to be independent of the spatial coordinate $x$. Then, one can easily check by substitution (Lipatnikov 2009b) that Eqs. (6.34) and (6.77) have the following exact analytical solution for the Reynolds-averaged combustion progress variable

$$\bar{c} = \frac{1}{2}\,\mathrm{erfc}\left(\xi\sqrt{\pi}\right) = \sqrt{\frac{1}{\pi}}\int_{\xi\sqrt{\pi}}^{\infty} e^{-\zeta^2} d\zeta, \tag{6.87}$$

where

$$\xi = \frac{x - x_f(t)}{\delta(t)}, \tag{6.88}$$

$$x_f(t) = x_{f,0} + \int_0^t U_t d\zeta, \tag{6.89}$$

$x_{f,0}$ is an initial flame position,

$$\delta_t^2 = 4\pi \int_0^t D_t d\zeta, \tag{6.90}$$

and the mean flame brush thickness is defined using the maximum gradient method, i.e.,

$$\delta_t \equiv \frac{1}{\max\left\{\left|\partial\bar{c}/\partial x\right|\right\}}. \tag{6.91}$$

Indeed, substitution of Eq. (6.87) into the state Eq. (6.34) and the mass balance Eq. (6.15) results in

$$-\frac{1}{\rho_u - \rho_b}\frac{d\bar{\rho}}{d\xi} = \frac{\bar{\rho}^2}{\rho_u\rho_b}\frac{d\tilde{c}}{d\xi} = \frac{d\bar{c}}{d\xi} = -\mathrm{e}^{-\pi\xi^2} \tag{6.92}$$

and

$$\frac{d}{d\xi}(\bar{\rho}\tilde{u}) = \left(U_t + \xi\frac{d\delta_t}{dt}\right)\frac{d\bar{\rho}}{d\xi}, \tag{6.93}$$

respectively. Integrating the latter equation from $\xi$ to infinity and using Eq. (6.92), we obtain

$$-\bar{\rho}\tilde{u} = U_t(\rho_u - \bar{\rho}) + \frac{d\delta_t}{dt}\int_{\xi}^{\infty}\zeta\frac{d\bar{\rho}}{d\zeta}d\zeta = U_t(\rho_u - \bar{\rho}) + \frac{d\delta_t}{dt}\frac{\rho_u - \rho_b}{2\pi}\mathrm{e}^{-\pi\xi^2} \tag{6.94}$$

in the framework linked with the unburned gas, i.e., $\tilde{u}(\xi \to \infty) \to 0$. Substitution of Eqs. (6.87) and (6.94) into Eq. (6.77) yields

$$-\bar{\rho}\xi\frac{d\delta_t}{dt}\frac{d\tilde{c}}{d\xi}-\rho_u U_t\frac{d\tilde{c}}{d\xi}-\frac{d\delta_t}{dt}\frac{\rho_u-\rho_b}{2\pi}\mathrm{e}^{-\pi\xi^2}\frac{d\tilde{c}}{d\xi}$$
$$=\frac{D_t}{\delta_t}\frac{d}{d\xi}\left(\bar{\rho}\frac{d\tilde{c}}{d\xi}\right)-\rho_u U_t\frac{d\tilde{c}}{d\xi}. \tag{6.95}$$

Using Eq. (6.92), we obtain

$$\frac{1}{2}\frac{d\delta_t^2}{dt}\frac{\rho_b}{\bar{\rho}^2}\frac{d\bar{c}}{d\xi}\left(-\bar{\rho}\xi+\frac{\rho_u-\rho_b}{2\pi}\frac{d\bar{c}}{d\xi}\right)$$
$$=D_t\frac{d}{d\xi}\left(\frac{\rho_b}{\bar{\rho}}\frac{d\bar{c}}{d\xi}\right)=D_t\frac{\rho_b}{\bar{\rho}^2}\left[(\rho_u-\rho_b)\frac{d\bar{c}}{d\xi}-2\pi\xi\bar{\rho}\right]\frac{d\bar{c}}{d\xi}, \tag{6.96}$$

which is valid if Eq. (6.90) holds. Thus, Eqs. (6.87)–(6.90) satisfy Eq. (6.77) supplemented with the state Eq. (6.35) and the mass balance Eq. (6.15).

It is worth noting that, in the above equations, the burning velocity $U_t$ may be evaluated using either Eq. (6.79) within the framework of the TFC model or Eq. (6.82) associated with the FSC model. Similarly, the diffusivity $D_t$ may either be constant within the framework of the TFC model or depend on flame-development time, e.g. see Eq. (6.81) associated with the FSC model.

This analytical solution reveals three important features of the TFC model. First, different terms on the RHS of Eq. (6.77) control different flame characteristics. The second spatial derivative in the turbulent diffusion term controls the shape of the spatial profile of $\bar{c}$. The turbulent diffusivity in the same term controls the growth of the mean flame brush thickness $\delta_t$, but does not affect the flame propagation speed, which is solely controlled by the gradient source term. On the contrary, the source term affects neither the mean flame structure nor the thickness $\delta_t$.

Second, the TFC model predicts self-similarity of the mean structure of a developing premixed turbulent flame, i.e., spatial profiles of $\bar{c}(x,t)$ collapse to the same curve $\bar{c}(\xi)$ if the spatial distance is normalized using the growing mean flame brush thickness, see Eq. (6.88).

Third, Eq. (6.90) yields a permanently growing mean flame brush thickness.

### 6.4.4 Validation

Let us begin with assessing the analytical results given by Eqs. (6.87) and (6.90). The self-similarity of the mean structure of a developing premixed turbulent flame is well documented in various experiments analyzed elsewhere (Lipatnikov and Chomiak 2000b, 2001, 2002, 2004), see also recent papers (Tamadonfar and Gülder 2014, 2015), with the measured self-similar profiles of $\bar{c}(\xi)$ being well fitted with Eq. (6.87), e.g., see Fig. 6.10.

As far as development of mean flame brush thickness is concerned, substitution of a constant $D_t \propto u'L$ associated with the TFC model into Eq. (6.90) yields

$$\delta_t \propto \sqrt{u'Lt}, \tag{6.97}$$

whereas substitution of Eq. (6.81) associated with the FSC model into Eq. (6.90) results in

$$\frac{\delta_t^2}{4\pi u'^2 \tau_L^2} = \theta_{fd}\left[1 - \frac{1}{\theta_{fd}}\left(1 - \mathrm{e}^{-\theta_{fd}}\right)\right] \tag{6.98}$$

and, hence, $\delta_t \propto u' t_{fd}$ at $\theta_{fd} = t_{fd}/\tau_L = t_{fd} u'^2 / D_{t,\infty} \ll 1$ and $\delta_t = 2u'\tau_L\sqrt{\pi\theta_{fd}} \propto \sqrt{u' L t_{fd}}$ at $\theta_{fd} \gg 1$. Consequently, the former model yields a significantly larger $\delta_t$ during an earlier stage of the flame development, but the mean flame brush thicknesses obtained using the two models are almost equal to one another at large $\theta_{fd}$, cf. solid and dashed lines in Fig. 6.11a.

Figure 6.11b indicates that results calculated using Eq. (6.98), see solid line, agree with various experimental data, see symbols, substantially better than results calculated using Eq. (6.97), see dashed line. Qualitatively, the TFC model yields square-root dependence of the mean flame brush thickness on the flame-development time, whereas the FSC model predicts the linear dependence of $\delta_t \propto u' t_{fd}$ at $t_{fd} \ll \tau_L$. The latter prediction is validated not only by the data plotted in Fig. 6.11b, but also by numerous other data obtained from various flames, e.g., see recent papers (Chowdhury and Cetegen 2017; Kheirkhah and Gülder 2013, 2014, 2015; Sponfeldner et al. 2015; Tamadonfar and Gülder 2014, 2015). Indeed, those data show (i) the linear dependence of $\delta_t$ on the distance from the flame-holder and, hence, on the flame-development time and (ii) and an almost linear increase in $\delta_t$ by $u'$.

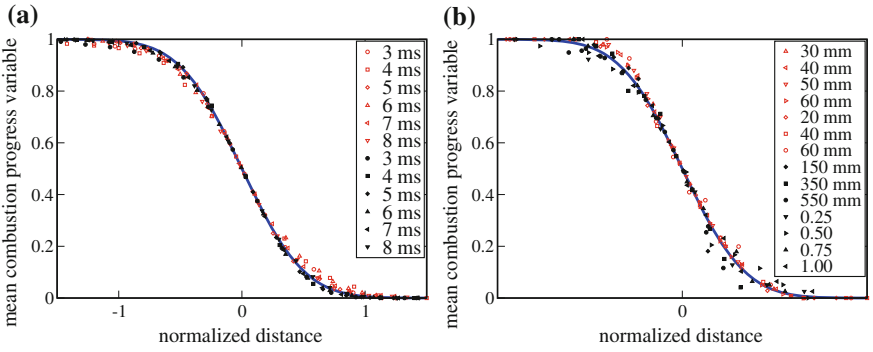


**Fig. 6.10** Self-similar profiles of the mean combustion progress variable. **a** Data obtained by Renou et al. (2002) from expanding statistically spherical lean ($\Phi = 0.27$) $H_2$-air (open symbols) and stoichiometric $C_3H_8$-air (filled symbols) flames under the room conditions at different instants after spark ignition, specified in legends. Curve shows results computed using Eq. (6.87). **b** Data obtained by Gouldin and Miles (1995) from lean ($\Phi = 0.68$) $C_2H_6$-air V-shaped flames (open triangles), by Namazian et al. (1986) from lean ($\Phi = 0.8$) $C_2H_6$-air V-shaped flames (open squares, diamonds, and circles), by Sjunnesson et al. (1992) from lean ($\Phi = 0.6$) $C_3H_8$-air confined flames stabilized with a bluff body (filled squares, diamonds, and circles), and by Wu et al. (1990) from lean ($\Phi = 0.8$) $H_2$-air jet flames (filled triangles). Dimensional or normalized distances from flame stabilization points are specified in legends. Curve shows results computed using Eq. (6.87)

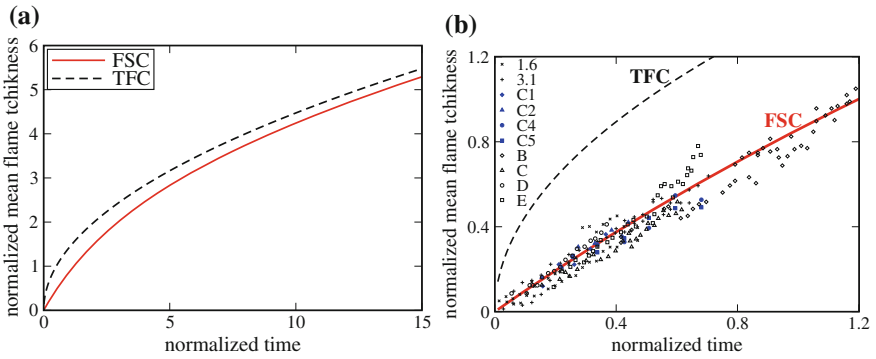


**Fig. 6.11** Normalized mean flame brush thickness $\delta_t/\sqrt{2\pi L}$ versus normalized flame-development time $\theta_{fd}$. **a**, **b** Dashed and solid lines show results calculated using Eqs. (6.97) and (6.98) associated with the TFC and FSC models, respectively. **b** Crosses and pluses show data obtained by Atashkari et al. (1999) from expanding statistically spherical $CH_4$-air flames at two different values of $u'/S_L$ specified in legends. Filled diamonds, triangles, circles and squares show data obtained by Renou et al. (2002) from expanding statistically spherical stoichiometric $CH_4$-air (C2, $u'/S_L = 0.92$ and C5, $u'/S_L = 1.38$) and $C_3H_8$-air (C1, $u'/S_L = 0.85$ and C4, $u'/S_L = 1.28$) flames. Open diamonds, triangles, circles, and squares show data obtained by Goix et al. (1990) from open V-shaped lean ($\Phi = 0.2$) $H_2$-air flames B, C, D, and E stabilized in different turbulent flows

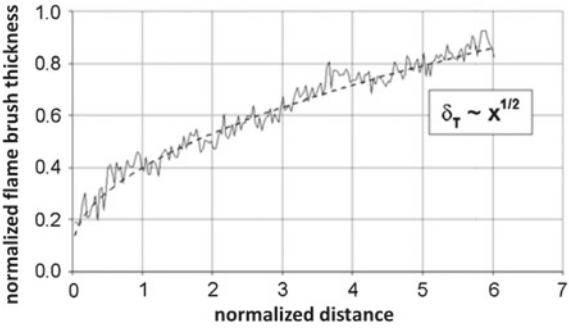


**Fig. 6.12** Growth of the normalized mean flame brush thickness with the normalized distance from the combustor inlet. Reprinted from the paper by Griebel et al. (2007)

It is worth noting that certain data obtained from V-shaped (Kheirkhah and Gülder 2013, 2014, 2015) or Bunsen (Tamadonfar and Gülder 2014, 2015) statistically stationary flames indicate an increase in a flame thickness $\Delta_t$ by $S_L$, with $\Delta_t$ being measured along a normal to the burner axis, rather than along a normal to the mean flame position. Since $U_t$ is increased by $S_L$, an acute angle $\varphi$ between the aforementioned axis and the mean flame surface is also increased by $S_L$. This effect can result in increasing $\Delta_t \approx \delta_t/\cos\varphi$ even if $\delta_t$ is constant.

Experimental data obtained from long flames and associated with a long flame-development time show the square-root dependence of $\delta_t$ on the distance from the flame-holder, e.g., see Fig. 6.12, in line with the TFC Eq. (6.97) or the FSC Eq. (6.98).

Let us consider results of testing the TFC and FSC models in RANS simulations of well-defined simple cases.

The TFC model has been shown to predict;

- The effects of mixture composition (the equivalence ratio and various fuels such as methane, ethane, propane, etc.) on turbulent burning velocities obtained from statistically spherical, premixed turbulent flames expanding in a fan-stirred bomb at various $u'$, e.g., see Fig. 6.13a. Comparison of curves shown in dashed ($\mathbb{P}_q = 0$) and solid ($0 < \mathbb{P}_q < 1$) lines in Fig. 6.13a indicates that the submodel for the quenching probability $\mathbb{P}_q$ given by Eq. (6.86) affects the computed results only at high $u'$. As far as the increasing branches of the measured and computed curves, associated with moderate turbulence, are concerned, the obtained good agreement between the experimental and the numerical data does not result from tuning of $\dot{s}_q$ in Eq. (6.86). In the case of the stoichiometric $C_3H_8$-air mixture, results computed either setting $\mathbb{P}_q = 0$ or using Eqs. (6.85) and (6.86) are almost the same. Accordingly, solely the former results are shown in a dashed line in this case.
- Mean structure of an open, Bunsen, premixed turbulent flame (Dinkelacker 2002).
- Profiles of the mean combustion progress variable in two open, swirl-stabilized flames (Dinkelacker 2002).
- Burning velocities obtained from slightly lean ($\Phi = 0.9$) $CH_4$-air Bunsen flames under normal and elevated pressures provided that a ratio of $u'/S_L$ is markedly lager than unity, cf. filled and open symbols at $(u'/S_L)(p_0/p) \geq 0.6$ in Fig. 6.13b. If the ratio of $u'/S_L$ is low, the TFC model underpredicts the measured data, because $U_{t,ISP}$ given by Eq. (6.79) tends to zero at $u' \to 0$.
- Mean structure of a statistically stationary, oblique, confined, lean ($\Phi = 0.8$) $CH_4$-air turbulent flame stabilized by a hot jet in intense turbulence (Ghirelli 2011; Yasari et al. 2015; Zimont et al. 2001), cf. dashed lines and symbols in Fig. 6.15d.
- Mean shape of open, V-shaped, lean ($\Phi = 0.5$, 0.58, and 0.7) $CH_4$-air turbulent flames (Dinkelacker and Hölzler 2000; Ghirelli 2011; Moreau 2009).
- Influence of bulk flow velocity, turbulence generation method, and pressure, on the mean axial length and the mean axial thickness of confined preheated ($T_u = 673$ K) lean ($\Phi = 0.5$) $CH_4$-air turbulent flames stabilized due to abrupt expansion of a channel at elevated pressures, cf. symbols and dashed lines in Fig. 6.13c and d.
- Axial profile of the Reynolds-averaged combustion progress variable in such a flame, see Fig. 6.13e.
- Mean shape of a lean ($\Phi = 0.7$) $CH_4$-air V-shaped flame, see Fig. 6.13f.

Moreover, the TFC model was successfully applied to RANS simulations of premixed and partially premixed turbulent combustion in engines, e.g., see (Polifke et al. 2002; Zimont et al. 1998).

Thus, the predictive capabilities of the TFC model were quantitatively validated by several independent research groups in RANS simulations of a wide set of substantially different, well-defined, simple premixed turbulent flames. Nevertheless, certain experimental results were not predicted in the numerical studies cited above.

First, to obtain a decrease in $U_t$ by $u'$ in intense turbulence, Eqs. (6.85) and (6.86) with unknown input parameter $\dot{s}_q$ were invoked, with $\dot{s}_q$ being tuned. Accordingly,

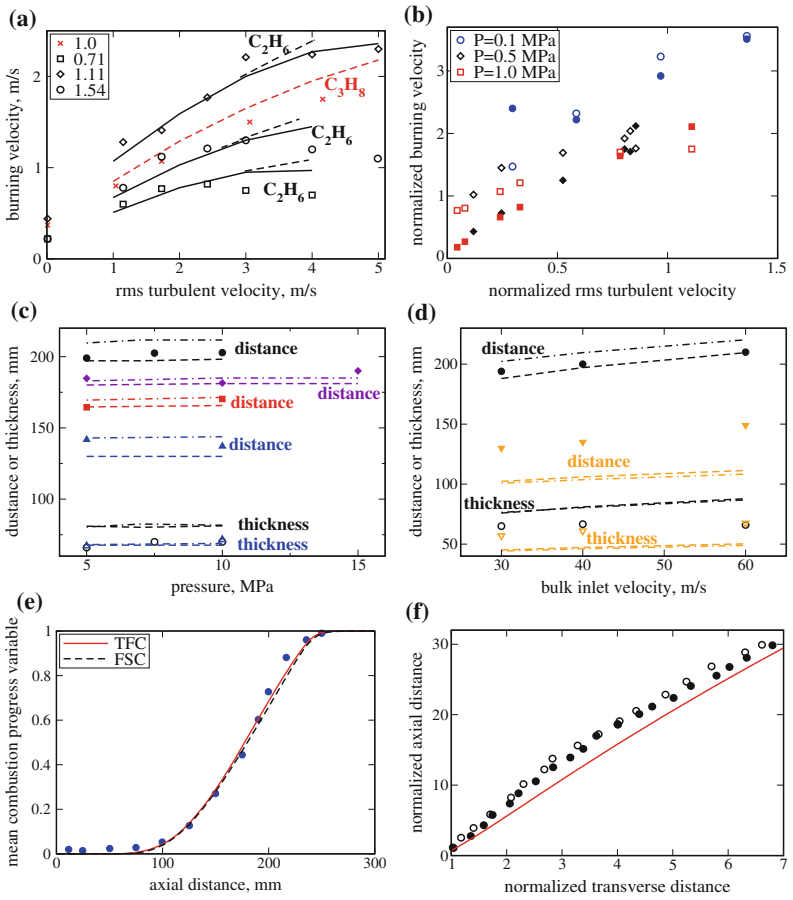


**Fig. 6.13** Some examples of validation of the TFC model with $A = 0.5$ in RANS simulations of various experiments. **a** Dependencies of turbulent burning velocity $U_t$ on the rms turbulent velocity $u'$ measured (symbols) by Karpov and Severin (1980) and computed (curves) by Karpov et al. (1996). Crosses show data obtained from $C_3H_8$-air flames. Other symbols show data obtained from $C_2H_6$-air flames. Equivalence ratio is specified in figure legends. Solid and dashed lines show results computed invoking Eq. (6.85) with a tuned $\dot{s}_q$ and Eq. (6.79), respectively. **b** Normalized turbulent burning velocities measured (open symbols) by Kobayashi et al. (1996) and computed (filled symbols) by Muppala and Dinkelacker (2004) at three different pressures specified in the legends. Both $U_t/S_L$ and $u'/S_L$ are multiplied with $p_0/p$ in order for the scales of the data obtained at different pressures to be comparable. $p_0 = 0.1$ MPa. **c**, **d** The mean centerline flame position (filled symbols) and the mean centerline flame brush thickness (open symbols) versus pressure and inlet bulk velocity, respectively. Different symbols show experimental data obtained by Siewert (2006) utilizing different grids in order to generate turbulence. Results computed by Yasari et al. (2015) using the TFC and FSC models are shown in dashed and dotted-dashed lines, respectively. **e** Centerline profiles of the Reynolds-averaged combustion progress variable, measured (symbols) by Siewert (2006) and computed by Yasari et al. (2015) using either the TFC (solid line) or FSC (dashed line) model. **f** Mean surface of a V-shaped flame. Open and filled symbols show experimental data obtained by Kheirkhah and Gülder (2013) from the left and right, respectively, branches of the flame. Line show results computed by Verma and Lipatnikov (2016)

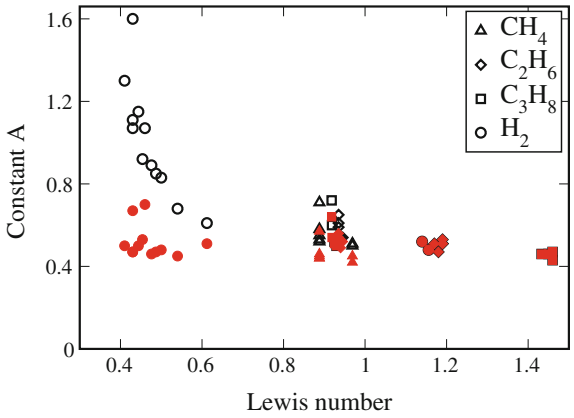


**Fig. 6.14** Values of $A$ tuned in RANS simulations (Karpov et al. 1996; Zimont and Lipatnikov 1995) of experiments by Karpov and Severin (1980) versus the Lewis number. Open symbols show results obtained using the original TFC model. Filled symbols show results obtained substituting the standard chemical time scale $\tau_c$ in Eq. (6.79) with a chemical time that characterizes local burning rate in extremely curved laminar flames

the so-extended TFC model cannot predict the decrease in $U_t$ by $u'$ in intense turbulence, but this phenomenon challenges all combustion models to the best of the present author's knowledge.

Second, the TFC model underpredicts $U_t$ in weak turbulence, e.g., see Fig. 6.13b. Moreover, Yasari et al. (2015) were not able to obtain reasonable agreement between numerical and measured data when applying the TFC model to RANS simulations of experiments with weakly turbulent Bunsen flames (Cohé et al. 2009; Pfadler et al. 2008), whereas the FSC model performs much better in these cases, as will be discussed later.

Third, in simulations of the flames investigated by Siewert (2006), the TFC model (i) underpredicted the influence of variations in $\Phi$ on the mean flame axial length and (ii) yielded too narrow radial profiles of $\bar{c}(r)$ when compared to the measured data (Yasari et al. 2015). In the cited paper, the observed difference between the measured and computed results was attributed to the influence of heat release on the turbulence and to eventual local combustion quenching.

Finally, it is worth noting that the original TFC model significantly underpredicts turbulent burning velocities obtained by Karpov and Severin (1980) from expanding, statistically spherical lean hydrogen flames. In particular, when the TFC model was applied to RANS simulations of similar flames propagating in hydrocarbon–air mixtures (Karpov et al. 1996; Zimont and Lipatnikov 1995), a reasonably good agreement with the experimental data was obtained using the same $A = 0.5$ for various mixtures, but the agreement could be improved by slightly tuning the value of $A$ in certain cases. However, the values of $A$ tuned in similar simulations of lean hydrogen flames are significantly larger than 0.5 and are increased with decreasing the Lewis number, see open symbols in Fig. 6.14. This trend vanishes if the standard

chemical time scale $\tau_c$ in Eq. (6.79) is substituted with a chemical time that characterizes local burning rate in extremely curved laminar flames, see filled symbols. The reader interested in further discussion and substantiation of such a method is referred to books (Kuznetsov and Sabelnikov 1990; Lipatnikov 2012) and a review paper (Lipatnikov and Chomiak 2005c).

The FSC model has been shown to predict;

- Dependence of the mean growth rate of a statistically spherical flame kernel on mixture composition, e.g. see Fig. 6.15a and b.
- Dependence of the mean growth rate of a statistically spherical flame kernel on the rms turbulent velocity, e.g., see Fig. 6.15a and b.
- An increase in the observed turbulent flame speed as the flame kernel grows, e.g., see Fig. 6.15c.
- An increase in the observed turbulent flame speed by pressure, e.g., see Fig. 6.15c.
- Mean structure of a statistically stationary, oblique, confined, lean ($\Phi = 0.8$) $CH_4$-air turbulent flame stabilized by a hot jet in intense turbulence, e.g., see Fig. 6.15d, which also shows that results computed using the FSC model agree with the experimental data better than results computed using the TFC model, cf. solid and dashed lines, respectively.
- Mean shape of open, V-shaped, lean ($\Phi = 0.5$, 0.58, and 0.7) $CH_4$-air turbulent flames, e.g., see Fig. 6.15e, which also shows that results computed using the FSC model agree with the experimental data better than results computed using the TFC model, cf. solid and dotted-dashed lines, respectively.
- Influence of bulk flow velocity, turbulence generation method, and pressure on the mean axial length and the mean axial thickness of confined preheated ($T_u = 673$ K) lean ($\Phi = 0.5$) $CH_4$-air turbulent flames stabilized due to abrupt expansion of a channel at elevated pressures, cf. symbols and dotted-dashed lines in Fig. 6.13c and d. When simulating these experiments, the TFC and FSC models yielded very close results, cf. dashed and dotted-dashed lines, respectively.
- Axial profile of the Reynolds-averaged combustion progress variable in such a flame, see Fig. 6.13e.
- Mean structure of confined lean ($\Phi = 0.61$) $C_3H_8$-air flames stabilized by a bluff body, e.g. see Fig. 6.15f, which also shows that results computed using the FSC model agree with the experimental data better than results computed using the TFC model, cf. solid and dashed lines, respectively.
- Mean axial heights of the leanest $CH_4$-air weakly turbulent Bunsen flames, measured by Pfadler et al. (2008) at various equivalence ratios or inlet mass flow rates, with the TFC model yielding unsatisfactory results in this case (Yasari et al. 2015).
- Axial profiles of $\bar{c}(x)$ obtained by Cohé et al. (2009) from axisymmetric weakly turbulent $CH_4/CO_2$/air Bunsen flames stabilized within a cylindrical high pressure combustion chamber using an annular laminar stoichiometric methane–air pilot flame, with the TFC model yielding unsatisfactory results in this case (Yasari et al. 2015).

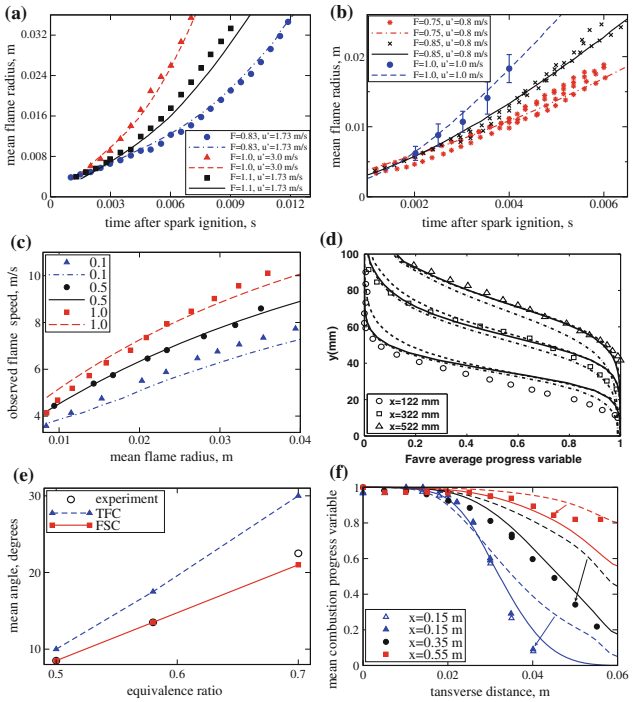


**Fig. 6.15** Some examples of validation of the FSC model with $\mathbb{P}_q = 0$ in RANS simulations of various experiments. **a** Increase in the mean radii of expanding statistically spherical $CH_4$-air turbulent flames. Symbols show Leeds experimental data (Bradley et al. 1994b) obtained at $L = 20$ mm and $T_u = 328$ K. Lines show results computed using the FSC model (Lipatnikov and Chomiak 1997; Lipatnikov et al. 1998). Equivalence ratio and $u'$ are specified in the legends. **b** Increase in the mean radii of expanding statistically spherical $C_3H_8$-air turbulent flames. Symbols show Rouen experimental data (Mouqallid et al. 1994) obtained at $L = 5$ mm and $T_u = 295$ K. Lines show results computed using the FSC model (Lipatnikov and Chomiak 1997; Lipatnikov et al. 1998). Equivalence ratio and $u'$ are specified in the legends. **c** Observed speeds $d\bar{R}_f/dt$ of expanding, statistically spherical, stoichiometric iso-octane/air turbulent flames versus the mean flame radius $\bar{R}_f$. Symbols show Leeds experimental data (Bradley et al. 1994a) obtained at $u' = 2$ m/s, $L = 20$ mm, and $T_u = 400$ K. Lines show results computed using the FSC model (Lipatnikov and Chomiak 1997). Pressure is specified in MPa in the legends. **d** Transverse profiles of $\tilde{c}(y)$, computed by Yasari et al. (2015) using the TFC model (dashed lines), the FSC model (solid lines), and the FSC model with $Q_L = 0$ (dotted-dashed lines). Symbols show experimental data obtained by Moreau (1977) at various distances $x$ from the inlet, specified in legends. Circles, squares, and triangles show data obtained from flames with $\Phi = 0.83$, 0.85, and 0.87, respectively. **e** Circles show an angle between the mean flame surface and the burner axis, averaged over $15 \le x \le 45$ mm in the experiments by Dinkelacker and Hölzler (2000). Triangles and squares show the mean angle computed by Yasari et al. (2015) using the TFC and FSC model, respectively. **f** Transverse profiles of the normalized Reynolds-averaged temperature. Symbols show experimental data (Sjunnesson et al. 1992) obtained from preheated ($T_u = 600$ K) lean ($\Phi = 0.61$) $C_3H_8$-air flames at different distances from a bluff body, specified in the legends. Data measured in the up and down halves of the channel are plotted in open and filled symbols, respectively. Dashed and solid lines show results (Sathiah and Lipatnikov 2007) computed using the TFC and FSC models, respectively

Thus, predictive capabilities of the FSC model were quantitatively validated in RANS simulations of a wide set of substantially different, well-defined, simple premixed turbulent flames. Nevertheless, certain experimental results were not predicted in the numerical studies cited above.

First, as already noted, in the simulations of the flames investigated by Siewert (2006), the FSC model (i) underpredicted the influence of variations in $\Phi$ on the mean flame axial length and (ii) yielded too narrow radial profiles of $\bar{c}(r)$ when compared to the measured data (Yasari et al. 2015). In the cited paper, the observed difference between the measured and computed results was attributed to the influence of heat release on the turbulence and to eventual local combustion quenching.

Second, in the simulations of the Bunsen flames investigated by Pfadler et al. (2008), the FSC model substantially underpredicted the axial flame height at $\Phi > 0.8$ and underpredicted the axial flame thickness in all studied cases (Yasari and Lipatnikov 2015). In the cited paper, the observed difference between the measured and computed results was also attributed to the influence of heat release on the turbulence.

It is also worth noting that the aforementioned RANS simulations of expanding and statistically stationary flames were performed using the FSC model with $A = 0.4$ and 0.5, respectively. In the former case, the value of $A$ was reduced, because the use of the extra term $Q_L$ was expected to result in increasing computed turbulent flame speed. Moreover, in the simulations by Sathiah and Lipatnikov (2007), the extra term $Q_L$ was skipped, but such a simplification appears to be justified in the case of a large ratio of $u'/S_L$ associated with that study.

Finally, it is worth noting that the FSC model was successfully applied to RANS simulations of stratified turbulent combustion in research optical SI engines (Huang et al. 2016; Wallesten et al. 2002).

## 6.5 Concluding Remarks

As shown in the present chapter, there are sufficiently advanced models, e.g., the TFC or FSC one, of the influence of turbulence on combustion that allow us to reasonably well predict mean turbulent burning rate, mean flame thickness and structure in various turbulent flows, for various fuels and equivalence ratios, at various pressures, etc.

Nevertheless, even the most advanced models cannot predict a decrease in turbulent burning velocity with increasing $u'$ in intense turbulence characterized by $u'/S_L \gg 1$ or $Ka > 1$. Such effects could be of great importance for burning of lean mixtures characterized by a low $S_L$.

Moreover, the influence of combustion-induced thermal expansion on turbulence in flames is not yet well studied and this issue strongly challenges the combustion community.

Furthermore, simulation of emissions from turbulent flames is a very important subject, which has been attracting paramount attention. However, it is worth stressing that the mean heat-release rate and the mean flame structure should be well pre-

dicted in order for simulations of emissions to yield satisfactory results. Therefore, at the present level of model development, the best way of attacking this problem appears to consist in (i) computation of fields of the mean temperature, density, etc., by invoking an advanced model that does not address emissions, but can predict the aforementioned fields, and (ii) subsequent simulation of emissions invoking another model at a post-processing stage. The choice of an appropriate emission model is beyond the scope of the present chapter.

**Acknowledgements** This work was supported by Swedish Research Council (VR), Swedish Energy Agency (EM), Swedish Gas Turbine Center (GTC), Chalmers Areas of Advance Transport and Energy, and Combustion Engine Research Center (CERC). The author is grateful to Profs. Chomiak, Karpov, Sabelnikov, and Zimont for valuable discussions.

## References

Abdel-Gayed RG, Al-Khishali KJ, Bradley D (1984) Turbulent burning velocities and flame straining in explosions. Proc R Soc Lond A 391:391–414

Atashkari K, Lawes M, Sheppard CGW, Woolley R (1999) Towards a general correlation of turbulent premixed flame wrinkling. In: Rodi W, Laurence D (eds) Engineering turbulence modelling and measurements 4. In: Proceedings of 4th International Symposium on Engineering Turbulence Modelling and Measurements, Ajaccio, Corsica, France, 24–26 May, 1999, pp 805–814

Bailly P, Champion M, Garreton D (1997) Counter-gradient diffusion in a confined turbulent premixed flame. Phys Fluids 9:766–775

Bilger RW, Pope SB, Bray KNC, Driscoll JF (2005) Paradigms in turbulent combustion research. Proc Combust Inst 30:21–42

Borghi R (1990) Turbulent premixed combustion: further discussions of the scales of fluctuations. Combust Flame 80:304–312

Boudier P, Henriot S, Poinsot T, Baritaud T (1992) A model for turbulent flame ignition and propagation in spark ignition engines. Proc Combust Inst 24:503–510

Boughanem H, Trouvé A (1998) The domain of influence of flame instabilities in turbulent premixed combustion. Proc Combust Inst 27:971–978

Bradley D (1992) How fast can we burn? Proc Combust Inst 24:247–262

Bradley D (2002) Problems of predicting turbulent burning rates. Combust Theory Model 6:361–382

Bradley D, Lau AKC, Lawes M (1992) Flame stretch rate as a determinant of turbulent burning velocity. Philos Trans R Soc Lond A 338:359–387

Bradley D, Lawes M, Sheppard CGW (1994a) Study of turbulence and combustion interaction: measurement and prediction of the rate of turbulent burning. Report, University of Leeds

Bradley D, Lawes M, Scott MJ, Mushi EMJ (1994b) Afterburning in spherical premixed turbulent explosions. Combust Flame 99:581–590

Bradley D, Gaskell PH, Gu XJ, Sedaghat A (2005) Premixed flamelet modelling: factors influencing the turbulent heat release rate source term and the turbulent burning velocity. Combust Flame 143:227–245

Bray KNC (1979) The interaction between turbulence and combustion. Proc Combust Inst 17:223–233

Bray KNC (1980) Turbulent flows with premixed reactants. In: Libby PA, Williams FA (eds) Turbulent reacting flows. Springer, Berlin

Bray KNC (1987) Methods of including realistic chemical reaction mechanisms in turbulent combustion models. In: Warnatz J, Jager W (ed) Complex chemical reaction systems. Mathematical modelling and simulation. Springer, Heidelberg

Bray KNC (1990) Studies of the turbulent burning velocity. Proc R Soc Lond A 431:315–335
Bray KNC (1995) Turbulent transport in flames. Proc R Soc Lond A 451:231–256
Bray KNC (1996) The challenge of turbulent combustion. Proc Combust Inst 26:1–26
Bray KNC, Moss JB (1977) A unified statistical model for the premixed turbulent flame. Acta Astronaut 4:291–319
Bray KNC, Cant RS (1991) Some applications of Kolmogorov's turbulence research in the field of combustion. Proc R Soc Lond A 434:217–240
Bray KNC, Libby PA, Moss JB (1985) Unified modeling approach for premixed turbulent combustion—Part I: General formulation. Combust Flame 61:87–102
Bray KNC, Champion M, Libby PA, Swaminathan N (2006) Finite rate chemistry and presumed PDF models for premixed turbulent combustion. Combust Flame 146:665–667
Brodkey RS (1967) The phenomena of fluid motions. Addison-Wesley Publishing Company, London
Burluka AA, Griffiths JF, Liu K, Orms M (2009) Experimental studies of the role of chemical kinetics in turbulent flames. Combust Explos Shock Waves 45:383–391
Candel S, Poinsot T (1990) Flame stretch and the balance equation for the flame area. Combust Sci Technol 170:1–15
Candel S, Veynante D, Lacas F, Maistret E, Darabiha N, Poinsot T (1990) Coherent flame model: applications and recent extensions. In: Larrouturou BE (ed) Advances in combustion modeling. World Scientific, Singapore
Cant RS, Pope SB, Bray KNC (1990) Modelling of flamelet surface-to-volume ratio in turbulent premixed combustion. Proc Combust Inst 23:809–815
Chakraborty N, Champion M, Mura A, Swaminathan N (2011) Scalar-dissipation-rate approach. In: Swaminathan N, Bray KNC (eds) Turbulent premixed flames. Cambridge University Press, Cambridge
Chaudhuri S, Akkerman V, Law CK (2011) Spectral formulation of turbulent flame speed with consideration of hydrodynamic instability. Phys Rev E 84:026322
Cheng RK, Shepherd IG (1991) The influence of burner geometry on premixed turbulent flame propagation. Combust Flame 85:7–26
Cheng WK, Diringer JA (1991) Numerical modelling of SI engine combustion with a flame sheet model. SAE Paper 910268
Cho P, Law CK, Cheng RK, Shepherd IG (1988) Velocity and scalar fields of turbulent premixed flames in stagnation flow. Proc Combust Inst 22:739–745
Choi CR, Huh KY (1998) Development of a coherent flamelet model for spark-ignited turbulent premixed flame in a closed vessel. Combust Flame 114:336–348
Chowdhury BR, Cetegen BM (2017) Experimental study of the effects of free stream turbulence on characteristics and flame structure of bluff-body stabilized conical lean premixed flames. Combust Flame 178:311–328
Clavin P (1985) Dynamical behavior of premixed flame fronts in laminar and turbulent flows. Prog Energy Combust Sci 11:1–59
Clavin P, Williams FA (1979) Theory of premixed-flame propagation in large-scale turbulence. J Fluid Mech 90:589–604
Cohé C, Chauveau C, Gökalp I, Kurtuluş DF (2009) $CO_2$ addition and pressure effects on laminar and turbulent lean premixed $CH_4$ air flames. Proc Combust Inst 32:1803–1810
Damköhler G (1940) Der einfuss der turbulenz auf die flammengeschwindigkeit in gasgemischen. Z Electrochem 46:601–652
Darrieus G (1938) Propagation d'un front de flamme. Presented at La Technique Moderne (Paris) and in 1945 at Congrés de Mećanique Appliqueé (Paris)
Dasgupta D, Sun W, Day M, Lieuwen T (2017) Effect of turbulence-chemistry interactions on chemical pathways for turbulent hydrogen-air premixed flames. Combust Flame 176:191–201
Dinkelacker F (2002) Numerical calculation of turbulent premixed flames with an efficient turbulent flame speed closure model. In: Breuer M, Durst F, Zenger C (eds) High-performance scientific and engineering computing. Lecture notes in computational science and engineering, vol 21, pp 81–88

Dinkelacker F, Hölzler S (2000) Investigation of a turbulent flame speed closure approach for premixed flame calculations. Combust Sci Technol 158:321–340
Duclos JM, Veynante D, Poinsot T (1993) A comparison of flamelet models for premixed turbulent combustion. Combust Flame 95:101–117
Fichot F, Lacas F, Veynante D, Candel S (1993) One-dimensional propagation of a premixed turbulent flame with a balance equation for the flame surface density. Combust Sci Technol 90:35–60
Fogla N, Creta F, Matalon M (2017) The turbulent flame speed for low-to-moderate turbulence intensities: Hydrodynamic theory vs. experiments. Combust Flame 175:155–169
Frank JH, Kalt PAM, Bilger RW (1999) Measurements of conditional velocities in turbulent premixed flames by simultaneous OH PLIF and PIV. Combust Flame 116:220–232
Ghirelli F (2011) Turbulent premixed flame model based on a recent dispersion model. Comput Fluids 44:369–376
Giovangigli V (1999) Multicomponent flow modeling. Springer, Berlin
Goix P, Paranthoen P, Trinité M (1990) A tomographic study of measurements in a V-shaped $H_2$-air flame and a Lagrangian interpretation of the turbulent flame brush thickness. Combust Flame 81:229–241
Gouldin FC, Miles PC (1995) Chemical closure and burning rates in premixed turbulent flames. Combust Flame 100:202–210
Goulier J, Comandini A, Halter F, Chaumeix N (2017) Experimental study on turbulent expanding flames of lean hydrogen/air mixtures. Proc Combust Inst 36:2823–2832
Griebel P, Siewert P, Jansohn P (2007) Flame characteristics of turbulent lean premixed methane/air flames at high-pressure: turbulent flame speed and flame brush thickness. Proc Combust Inst 31:3083–3090
Hinze JO (1975) Turbulence, 2nd edn. McGraw Hill, New York
Hirschfelder JO, Curtiss CF, Bird RB (1954) Molecular theory of gases and liquids. Wiley, New York
Huang C, Yasari E, Johansen LCR, Hemdal S, Lipatnikov AN (2016) Application of flame speed closure model to RANS simulations of stratified turbulent combustion in a gasoline direct-injection spark-ignition engine. Combust Sci Technol 188:98–131
Karlovitz B, Denniston DW, Wells FE (1951) Investigation of turbulent flames. J Chem Phys 19:541–547
Karpov VP, Severin ES (1980) Effects of molecular-transport coefficients on the rate of turbulent combustion. Combust Explos Shock Waves 16:41–46
Karpov VP, Lipatnikov AN (1995) An effect of molecular thermal conductivity and diffusion on premixed combustion. Doklady Phys Chemistry 341:83–85
Karpov VP, Lipatnikov AN, Zimont, (1996) A test of an engineering model of premixed turbulent combustion. Proc Combust Inst 26:249–257
Karpov VP, Lipatnikov AN, Zimont (1997) Flame curvature as a determinant of preferential diffusion effects in premixed turbulent combustion. In: Sirignano WA, Merzhanov AG, De Luca L (eds) Advances in combustion science: In honor of Ya.B. Zel'dovich. Prog Astronaut Aeronaut 173:235-250
Kha KQN, Robin V, Mura A, Champion M (2016) Implications of laminar flame finite thickness on the structure of turbulent premixed flames. J Fluid Mech 787:116–147
Kheirkhah S, Gülder ÖL (2013) Turbulent premixed combustion in V-shaped flames: characteristics of flame front. Phys Fluids 25:055107
Kheirkhah S, Gülder ÖL (2014) Influence of edge velocity on flame front position and displacement speed in turbulent premixed combustion. Combust Flame 161:2614–2626
Kheirkhah S, Gülder ÖL (2015) Consumption speed and burning velocity in counter-gradient and gradient diffusion regimes of turbulent premixed combustion. Combust Flame 162:1422–1439
Kim SH (2017) Leading points and heat release effects in turbulent premixed flames. Proc Combust Inst 36:2017–2024
Kobayashi H, Tamura T, Maruta K, Niioka T, Williams FA (1996) Burning velocity of turbulent premixed flames in a high-pressure environment. Proc Combust Inst 26:389–396

Kuznetsov VR (1975) Certain peculiarities of movement of a flame front in a turbulent flow of homogeneous fuel mixtures. Combust Explos Shock Waves 11:487–493
Kuznetsov VR, Sabelnikov VA (1990) Turbulence and combustion. Hemisphere Publ Corp, New York
Landau LD (1944) On the theory of slow combustion. Acta Psysicochim USSR 19:77–85
Lapointe S, Blanquart G (2016) Fuel and chemistry effects in high Karlovitz premixed turbulent flames. Combust Flame 167:294–307
Launder BE, Spalding DB (1972) Mathematical models of turbulence. Academic Press, London
Law CK (2006) Combustion physics. Cambridge University Press, Cambridge
Lee B, Choi CR, Huh KY (1998) Application of the coherent flamelet model to counterflow turbulent premixed combustion and extinction. Combust Sci Technol 138:1–25
Li SC, Libby PA, Williams FA (1994) Experimental investigation of a premixed flame in an impinging turbulent stream. Proc Combust Inst 25:1207–1214
Libby PA (1975) On the prediction of intermittent turbulent flows. J Fluid Mech 68:273–295
Libby PA, Bray KNC (1977) Variable density effects in premixed turbulent flames. AIAA J 15:1186–1193
Libby PA, Bray KNC (1981) Countergradient diffusion in premixed turbulent flames. AIAA J 19:205–213
Libby PA, Williams FA (1994) Fundamental aspects and a review. In: Libby PA, Williams FA (eds) Turbulent reactive flows. Academic Press, London
Lindstedt RP, Váos EM (1999) Modeling of premixed turbulent flames with second moment methods. Combust Flame 116:461–485
Lipatnikov AN (2009a) Can we characterize turbulence in premixed flames? Combust Flame 156:1242–1247
Lipatnikov AN (2009b) Testing premixed turbulent combustion models by studying flame dynamics. Int J Spray Combust Dyn 1:39–66
Lipatnikov AN (2011a) Conditioned moments in premixed turbulent reacting flows. Proc Combust Inst 33:1489–1496
Lipatnikov AN (2011b) Transient behavior of turbulent scalar transport in premixed flames. Flow Turbul Combust 86:609–637
Lipatnikov AN (2012) Fundamentals of premixed turbulent combustion. CRC Press, Boca-Raton, Florida
Lipatnikov AN, Chomiak J (1997) A simple model of unsteady turbulent flame propagation. SAE Paper 972993
Lipatnikov AN, Chomiak J (2000a) Transient and geometrical effects in expanding turbulent flames. Combust Sci Technol 154:75–117
Lipatnikov AN, Chomiak J (2000b) Dependence of heat release on the progress variable in premixed turbulent combustion. Proc Combust Inst 28:227–234
Lipatnikov AN, Chomiak J (2001) Developing premixed turbulent flames: Part I. A self-similar regime of flame propagation. Combust Sci Technol 162:85–112
Lipatnikov AN, Chomiak J (2002) Turbulent flame speed and thickness: phenomenology, evaluation, and application in multi-dimensional simulations. Prog Energy Combust Sci 28:1–74
Lipatnikov AN, Chomiak J (2004) Comment on "Turbulent burning velocity, burned gas distribution, and associated flame surface definition" Bradley D, Haq MZ, Hicks RA, Kitagawa T, Lawes M, Sheppard CGW, Woolley R, Combust Flame, 133:415 (2003). Combust Flame 137:261–263
Lipatnikov AN, Chomiak J (2005a) A theoretical study of premixed turbulent flame development. Proc Combust Inst 30:843–850
Lipatnikov AN, Chomiak J (2005b) Self-similarly developing, premixed, turbulent flames: a theoretical study. Phys Fluids 17:065105
Lipatnikov AN, Chomiak J (2005c) Molecular transport effects on turbulent flame propagation and structure. Prog Energy Combust Sci 31:1–73
Lipatnikov AN, Sathiah P (2005) Effects of turbulent flame development on thermoacoustic oscillations. Combust Flame 142:130–139

Lipatnikov AN, Chomiak J (2010) Effects of premixed flames on turbulence and turbulent scalar transport. Prog Energy Combust Sci 36:1–102
Lipatnikov AN, Wallesten J, Nisbet J (1998) Testing of a model for multi-dimensional computations of turbulent combustion in spark ignition engines. In: Proc Fourth Int Symp Diagnostics and modeling of combustion in internal combustion engines—COMODIA98. JSME, Kyoto, pp 239–44
Lipatnikov AN, Nishiki S, Hasegawa T (2015a) DNS assessment of relation between mean reaction and scalar dissipation rates in the flamelet regime of premixed turbulent combustion. Combust Theory Model 19:309–328
Lipatnikov AN, Chomiak J, Sabelnikov VA, Nishiki S, Hasegawa T (2015b) Unburned mixture fingers in premixed turbulent flames. Proc Combust Inst 35:1401–1408
Lipatnikov AN, Sabelnikov VA, Nishiki S, Hasegawa T, Chakraborty N (2015c) DNS assessment of a simple model for evaluating velocity conditioned to unburned gas in premixed turbulent flames. Flow Turbul Combust 94:513–526
Lipatnikov AN, Sabelnikov VA, Nishiki S, Hasegawa T (2017) Flamelet perturbations and flame surface density transport in weakly turbulent premixed combustion. Combust Theory Model 21:205–227
Majda A, Sethian J (1985) The derivation and numerical solution of the equations for zero Mach number combustion. Combust Sci Technol 42:185–205
Meneveau C, Poinsot T (1991) Stretching and quenching of flamelets in premixed turbulent combustion. Combust Flame 86:311–332
Moreau P (1977) Turbulent flame development in a high velocity premixed flow. AIAA paper 77/49
Moreau V (2009) A self-similar premixed turbulent flame model. Appl Math Model 33:835–851
Moss JB (1980) Simultaneous measurements of concentration and velocity in an open premixed turbulent flame. Combust Sci Technol 22:119–129
Mouqallid M, Lecordier B, Trinité M (1994) High speed laser tomography analysis of flame propagation in a simulated internal combustion engine—applications to nonuniform mixture. SAE paper 941990
Muppala SRP, Dinkelacker F (2004) Numerical modelling of the pressure dependent reaction source term for turbulent premixed methane-air flames. Prog Comp Fluid Dyn 4:328–336
Namazian M, Shepherd IG, Talbot L (1986) Characterization of the density fluctuations in turbulent V-shaped premixed flames. Combust Flame 64:299–308
van Oijen JA, Donini A, Bastiaans RJM, ten Thije Boonkkamp JHM, de Goey LPH (2016) State-of-the-art in premixed combustion modeling using flamelet generated manifolds. Prog Energy Combust Sci 57:30–74
Peters N (2000) Turbulent combustion. The University Press, Cambridge
Pfadler S, Leipertz A, Dinkelacker F (2008) Systematic experiments on turbulent premixed Bunsen flames including turbulent flux measurements. Combust Flame 152:616–631
Poinsot T, Veynante D (2005) Theoretical and numerical combustion, 2nd edn. Edwards, Philadelphia
Poinsot T, Veynante D, Candel S (1991) Quenching processes and premixed turbulent combustion diagrams. J Fluid Mech 228:561–606
Polifke W, Flohr P, Brandt M (2002) Modeling of inhomogeneously premixed combustion with an extended TFC model. ASME J Eng Gas Turbines Power 124:58–65
Poludnenko AY, Oran ES (2011) The interaction of high-speed turbulence with flames: turbulent flame speed. Combust Flame 158:301–326
Pope SB (1988) The evolution of surface in turbulence. Int J Eng Sci 26:445–469
Pope SB (2000) Turbulent flows. The University Press, Cambridge
Prudnikov AG (1960) Hydrodynamics equations in turbulent flames. In: Prudnikov AG (ed) Combustion in a turbulent flow. Oborongiz, Moscow (in Russian)
Prudnikov AG (1964) Burning of homogeneous fuel-air mixtures in a turbulent flow. In: Raushenbakh BV (ed) Physical principles of the working process in combustion chambers of jet engines. Mashinostroenie, Moscow (in Russian; translated from Russian by the Translation Division, For-

eign and Technology Division, Wright Patterson AFB, Clearing House for Federal Scientific & Technical Information, Ohio, 1967, pp 244–336)
Renou B, Mura A, Samson E, Boukhalfa A (2002) Characterization of the local flame structure and flame surface density for freely-propagating premixed flames at various Lewis numbers. Combust Sci Technol 174:143–179
Roberts WL, Driscoll JF, Drake MC, Goss LP (1993) Images of the quenching of a flame by a vortex—to quantify regimes of turbulent combustion. Combust Flame 94:58–69
Sabelnikov VA, Lipatnikov AN (2011) A simple model for evaluating conditioned velocities in premixed turbulent flames. Combust Sci Technol 183:588–613
Sabelnikov VA, Lipatnikov AN (2013) Transition from pulled to pushed premixed turbulent flames due to countergradient transport. Combust Theory Model 17:1154–1175
Sabelnikov VA, Lipatnikov AN (2015) Transition from pulled to pushed fronts in premixed turbulent combustion: theoretical and numerical study. Combust Flame 162:2893–2903
Sabelnikov VA, Lipatnikov AN (2017) Recent advances in understanding of thermal expansion effects in premixed turbulent flames. Annu Rev Fluid Mech 49:91–117
Sabelnikov VA, Lipatnikov AN, Chakraborty N, Nishiki S, Hasegawa T (2016) A transport equation for reaction rate in turbulent flows. Phys Fluids 28:081701
Sabelnikov VA, Lipatnikov AN, Chakraborty N, Nishiki S, Hasegawa T (2017) A balance equation for the mean rate of product creation in premixed turbulent flames. Proc Combust Inst 36:1893–1901
Sathiah P, Lipatnikov AN (2007) Effects of flame development on stationary premixed turbulent combustion. Proc Combust Inst 31:3115–3122
Schmidt HP, Habisreuther P, Leuckel W (1998) A model for calculating heat release in premixed turbulent flames. Combust Flame 113:79–91
Scurlock AC, Grover JH (1953) Propagation of turbulent flames. Proc Combust Inst 4:645–658
Shelkin KI (1943) On combustion in a turbulent flow. J Tech Phys 13:520–530. Transl NACA, 1967, in NACA TM 1110:1–18 (from Russian)
Siewert P (2006) Flame front characteristics of turbulent lean premixed methane/air flames at high-pressure. PhD thesis, ETHZ Zürich
Sjunnesson A, Henrikson, Löfström C (1992) CARS measurements and visualization of reacting flows in a bluff body stabilized flame. AIAA paper 92/3650
Sponfeldner T, Soulopoulos N, Beyrau F, Hardalupas Y, Taylor AMKP, Vassilicos JC (2015) The structure of turbulent flames in fractal- and regular-grid-generated turbulence. Combust Flame 162:3379–3393
Stevens EJ, Bray KNC, Lecordier B (1998) Velocity and scalar statistics for premixed turbulent stagnation flames using PIV. Proc Combust Inst 27:949–955
Swaminathan N, Bray KNC (2005) Effect of dilatation on scalar dissipation in turbulent premixed flames. Combust Flame 143:549–565
Taylor GI (1935) Statistical theory of turbulence. IV. Diffusion in a turbulent air stream. Proc R Soc Lond A 151:465–478
Tamadonfar P, Gülder ÖL (2014) Flame brush characteristics and burning velocities of premixed turbulent methane/air Bunsen flames. Combust Flame 161:3154–3165
Tamadonfar P, Gülder ÖL (2015) Effects of mixture composition and turbulence intensity on flame front structure and burning velocities of premixed turbulent hydrocarbon/air Bunsen flames. Combust Flame 162:4417–4441
Townsend AA (1976) The structure of turbulent shear flow, 2nd edn. Cambridge University Press, Cambridge
Trouvé A, Poinsot T (1994) Evolution equation for flame surface density in turbulent premixed combustion. J Fluid Mech 278:1–31
Venkateswaran P, Marshall A, Shin DH, Noble D, Seitzman J, Lieuwen T (2011) Measurements and analysis of turbulent consumption speeds of $H_2$/CO mixtures. Combust Flame 158:1602–1614
Venkateswaran P, Marshall A, Seitzman J, Lieuwen T (2013) Pressure and fuel effects on turbulent consumption speeds of $H_2$/CO blends. Proc Combust Inst 34:1527–1535

Venkateswaran P, Marshall A, Seitzman J, Lieuwen T (2015) Scaling turbulent flame speeds of negative Markstein length fuel blends using leading points concepts. Combust Flame 162:375–387

Verma S, Lipatnikov AN (2016) Does sensitivity of measured scaling exponents for turbulent burning velocity to flame configuration prove lack of generality of notion of turbulent burning velocity? Combust Flame 173:77–88

Vervisch L, Bidaux E, Bray KNC, Kollmann W (1995) Surface densiuty function in premixed turbulent combustion modeling, similarities between probability density function and flame surface approaches. Phys Fluids 7:2496–2503

Veynante D, Vervisch L (2002) Turbulent combustion modeling. Prog Energy Combust Sci 28:193–266

Wallesten J, Lipatnikov AN, Chomiak J (2002) Modeling of stratified combustion in a DI SI engine using detailed chemistry pre-processing. Proc Combust Inst 29:703–709

Wang Z, Magi V, Abraham J (2017) Turbulent flame speed dependencies of lean methane-air mixtures under engine relevant conditions. Combust Flame 180:53–62

Williams FA (1985) Combustion theory, 2nd edn. Benjamin/Cummings, Menlo Park, California

Wu MS, Kwon A, Driscoll G, Faeth GM (1990) Turbulent premixed hydrogen/air flames at high Reynolds numbers. Combust Sci Technol 73:327–350

Yanagi T, Mimura Y (1981) Velocity-temperature correlation in premixed flame. Proc Combust Inst 18:1031–1039

Yasari E, Lipatnikov AN (2015) Assessment of a recent model of turbulent scalar flux in RANS simulations of premixed Bunsen flames. In: Hanjalic K, Miyauchi T, Borello D, Hadžiabdić M, Venturini P (eds) THMT15, Proceedings of the International Symposium Turbulence, Heat and Mass Transfer 8, Sarajevo, Bosnia and Herzegovina, September 15–18, 2015. ICHMT

Yasari E, Verma S, Lipatnikov AN (2015) RANS simulations of statistically stationary premixed turbulent combustion using flame speed closure model. Flow Turbul Combust 94:381–414

Yu R, Lipatnikov AN (2017a) A direct numerical simulation study of statistically stationary propagation of reaction wave in homogeneous turbulence. Phys Rev E 95:063101

Yu R, Lipatnikov AN (2017b) DNS study of dependence of bulk consumption velocity in a constant-density reacting flow on turbulence and mixture characteristics. Phys Fluids 29:065116

Yu R, Lipatnikov AN, Bay XS (2014) Three-dimensional direct numerical simulation study of conditioned moments associated with front propagation in turbulent flows. Phys Fluids 26:085104

Yu R, Bay XS, Lipatnikov AN (2015) A direct numerical simulation study of interface propagation in homogeneous turbulence. J Fluid Mech 772:127–164

Zel'dovich YaB, Barenblatt GI, Librovich VB, Makhviladze GM (1985) The mathematical theory of combustion and explosions. Consultants Bureau, New York

Zimont VL (1979) Theory of turbulent combustion of a homogeneous fuel mixture at high Reynolds number. Combust Explos Shock Waves 15:305–311

Zimont VL (2000) Gas premixed combustion at high turbulence. Turbulent flame closure combustion model. Exp Thermal Fluid Sci 21:179–186

Zimont VL (2015) Unclosed Favre-averaged equation for the chemical source and an analytical formulation of the problem of turbulent premixed combustion in the flamelet regime. Combust Flame 162:874–875

Zimont VL, Lipatnikov AN (1993) Calculation of the rate of heat release in a turbulent flame. Doklady Phys Chem 332:440–443

Zimont VL, Lipatnikov AN (1995) A numerical model of premixed turbulent combustion. Chem Phys Rep 14:993–1025

Zimont VL, Biagioli F, Syed K (2001) Modelling turbulent premixed combustion in the intermediate steady propagation regime. Prog Comput Fluid Dyn 1:14–28

Zimont VL, Polifke W, Bettelini M, Weisenstein W (1998) An efficient computational model for premixed turbulent combustion at high Reynolds number based on a turbulent flame speed closure. J Eng Gas Turbines Power 120:526–532